Cell

Pan-ebolavirus protective therapy by two multifunctional human antibodies

Graphical abstract

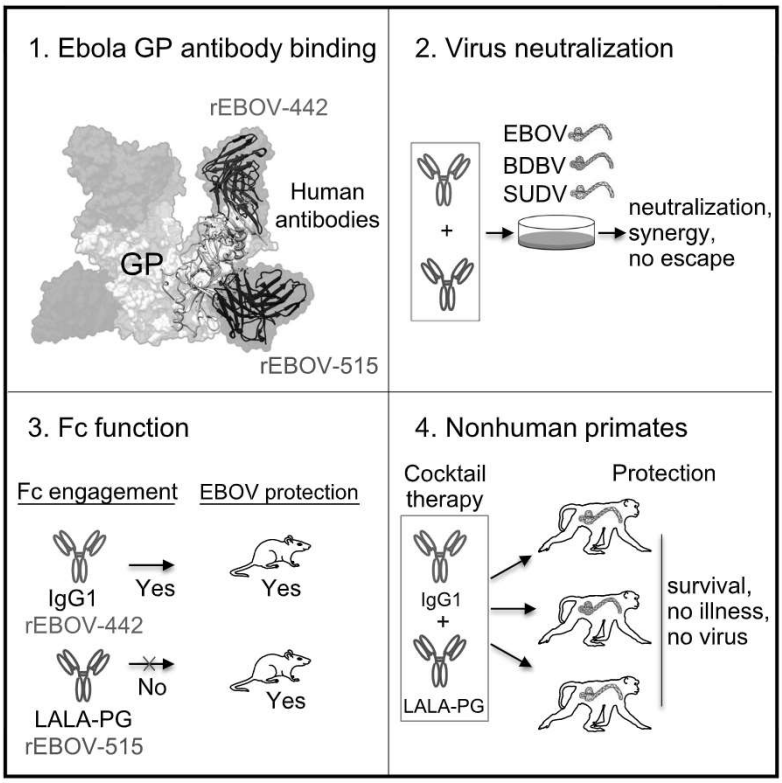

Highlights

- Two human antibodies recognize different conserved sites on ebolavirus glycoproteins
- The cocktail exhibits broad neutralizing activity and resists viral escape *in vitro*
- Antibodies synergize to neutralize virus and differentially engage their Fc regions
- The therapeutic cocktail protects NHPs against three medically important ebolaviruses

Authors

Pavlo Gilchuk, Charles D. Murin, Robert W. Cross, ..., Thomas W. Geisbert, Andrew B. Ward, James E. Crowe, Jr.

Correspondence

james.crowe@vumc.org

In brief

A broad-spectrum therapeutic antibody treatment against medically important ebolaviruses is not available but highly desirable. Gilchuk et al. report a therapeutic cocktail comprising two broadly neutralizing human antibodies that exhibit synergistic neutralizing activity, complementary Fc region-mediated effector functions, resistance to viral escape, and protection of non-human primates from disease caused by Ebola, Bundibugyo, or Sudan ebolaviruses with high effectiveness and also define the structural basis for neutralization breadth and potency by this cocktail.

Gilchuk et al., 2021, Cell *184*, 5593–5607
October 28, 2021
https://doi.org/10.1016/j.cell.2021.09.035

Cell

CellPress

Article

Pan-ebolavirus protective therapy by two multifunctional human antibodies

Pavlo Gilchuk,[1,8] Charles D. Murin,[2,8] Robert W. Cross,[3,4,8] Philipp A. Ilinykh,[3,5] Kai Huang,[3,5] Natalia Kuzmina,[3,5] Viktoriya Borisevich,[3,4] Krystle N. Agans,[3,4] Joan B. Geisbert,[3,4] Seth J. Zost,[1] Rachel S. Nargi,[1] Rachel E. Sutton,[1] Naveenchandra Suryadevara,[1] Robin G. Bombardi,[1] Robert H. Carnahan,[1,7] Alexander Bukreyev,[3,4,5] Thomas W. Geisbert,[3,4] Andrew B. Ward,[2] and James E. Crowe, Jr.[1,6,7,9,10,*]

[1]Vanderbilt Vaccine Center, Vanderbilt University Medical Center, Nashville, TN 37232, USA
[2]Department of Integrative Structural and Computational Biology, The Scripps Research Institute, La Jolla, CA 92037, USA
[3]Galveston National Laboratory, Galveston, TX 77550, USA
[4]Department of Microbiology and Immunology, University of Texas Medical Branch, Galveston, TX 77555, USA
[5]Department of Pathology, University of Texas Medical Branch, Galveston, TX 77555, USA
[6]Department of Pathology, Microbiology, and Immunology, Vanderbilt University Medical Center, Nashville, TN 37232, USA
[7]Department of Pediatrics, Vanderbilt University Medical Center, Nashville, TN 37232, USA
[8]These authors contributed equally
[9]Senior author
[10]Lead contact
*Correspondence: james.crowe@vumc.org
https://doi.org/10.1016/j.cell.2021.09.035

SUMMARY

Ebolaviruses cause a severe and often fatal illness with the potential for global spread. Monoclonal antibody-based treatments that have become available recently have a narrow therapeutic spectrum and are ineffective against ebolaviruses other than Ebola virus (EBOV), including medically important Bundibugyo (BDBV) and Sudan (SUDV) viruses. Here, we report the development of a therapeutic cocktail comprising two broadly neutralizing human antibodies, rEBOV-515 and rEBOV-442, that recognize non-overlapping sites on the ebolavirus glycoprotein (GP). Antibodies in the cocktail exhibited synergistic neutralizing activity, resisted viral escape, and possessed differing requirements for their Fc-regions for optimal *in vivo* activities. The cocktail protected non-human primates from ebolavirus disease caused by EBOV, BDBV, or SUDV with high therapeutic effectiveness. High-resolution structures of the cocktail antibodies in complex with GP revealed the molecular determinants for neutralization breadth and potency. This study provides advanced preclinical data to support clinical development of this cocktail for pan-ebolavirus therapy.

INTRODUCTION

The genus *Ebolavirus* consists of six antigenically distinct species, including Zaire ebolavirus (represented by Ebola virus [EBOV]), Sudan ebolavirus (Sudan virus [SUDV]), Bundibugyo ebolavirus (Bundibugyo virus [BDBV]), Taï Forest ebolavirus (Taï Forest virus [TAFV]), Reston ebolavirus (Reston virus [RESV]) (Feldmann et al., 2020; Kuhn et al., 2019), and Bombali ebolavirus (Bombali virus [BOMV]) (Goldstein et al., 2018). Three ebolaviruses—EBOV, BDBV, and SUDV—are responsible for severe disease and occasional deadly outbreaks in Africa posing a significant health threat and highlighting the urgent need for development of medical countermeasures. A total of 19 confirmed ebolavirus disease (EVD) outbreaks caused by EBOV have occurred, with >30,000 people infected to date and an average reported mortality rate of ~70% (World Health Organization, 2021). In 2021, there are ongoing EVD outbreaks in the Democratic Republic of the Congo (DRC) and Guinea (World Health Organization, 2021). BDBV has caused two confirmed outbreaks and infected 206 people (~32% mortality rate), and SUDV has been responsible for eight confirmed outbreaks and infected 779 people (~53% mortality rate) (World Health Organization, 2021). Monoclonal antibody (mAb) therapies have demonstrated safe and significant survival benefits in the treatment of acute EVD caused by EBOV in human trials (Gaudinski et al., 2019; Levine, 2019; Mulangu et al., 2019; Sivapalasingam et al., 2018), and several investigational human mAb treatments have been shown to reverse the advanced EVD in non-human primates caused by EBOV (Bornholdt et al., 2019; Corti et al., 2016; Gilchuk et al., 2020b; Pascal et al., 2018; Qiu et al., 2014), BDBV (Bornholdt et al., 2019; Gilchuk et al., 2018b), or SUDV (Bornholdt et al., 2019; Herbert et al., 2020). By 2020, two mAb-based therapeutics—ansuvimab-zykl (Ebanga) and atoltivimab + maftivimab + odesivimab-ebgn (Inmazeb)—have been developed and approved by the

Food and Drug Administration (FDA) for clinical use (Food and Drug Administration, 2020a, 2020b). Both of these approved mAb treatments are monospecific to EBOV and therefore not indicated for treatment of BDBV or SUDV infection. Identification of mAbs that cross-neutralize EBOV, BDBV, and SUDV with high potency is challenging due to the relatively high antigenic variability between these viruses (King et al., 2019). The efficacy of previously reported investigational mAb therapeutics typically is limited to only one of the three medically important ebolavirus species. The nature of future ebolavirus outbreaks cannot be predicted, however, and in a scenario of global spread, viruses can mutate rapidly making available mAb treatments vulnerable to escape, as has been recently shown for severe acute respiratory syndrome coronavirus 2 (SARS-CoV-2) (Starr et al., 2021; Wang et al., 2021). One approach could be to develop separate therapeutic mAb products for BDBV or SUDV or future escape variants of EBOV. It is desirable from a practical standpoint, however, to identify a single broad therapeutic spectrum mAb treatment of an equivalent or higher potency to existing monospecific mAb treatments that could be used for treatment of EBOV, BDBV, or SUDV. Therefore, ongoing efforts are needed to increase the therapeutic breadth of mAb therapies while maintaining or improving efficacy.

The ebolavirus envelope glycoprotein (GP) is the key target for neutralizing mAbs (King et al., 2018; Lee et al., 2008; Lee and Saphire, 2009; Misasi and Sullivan, 2021). We previously described isolation of two broadly neutralizing human mAbs, EBOV-515 and EBOV-442, using a human B cell hybridoma approach (Gilchuk et al., 2018a). Each of these two mAbs exhibited favorable immunological profiles, which included (1) broad reactivity for binding to GP of diverse species, (2) broad neutralization of authentic ebolaviruses (EBOV, BDBV, and SUDV), (3) recognition of distinct, non-overlapping epitopes in the GP (EBOV-515 is base-specific and EBOV-442 is glycan-cap-specific), and (4) a high level of therapeutic protection against EBOV. The antibodies EBOV-515 or EBOV-442 are analogous to the broadly reactive mAb EBOV-520 (GP-base-specific mAb) or mAb EBOV-548 (glycan-cap-specific), respectively (Gilchuk et al., 2018a, 2020b). We recently described a beneficial feature of the combination of EBOV-520 + EBOV-548 by showing that these two mAbs synergized for virus neutralization when combined in a cocktail and conferred therapeutic protection in EBOV-challenged rhesus macaques (Gilchuk et al., 2020b). We did not previously characterize the similar combination of EBOV-515 + EBOV-442. However, our previous studies revealed that the individual mAbs, EBOV-515 and EBOV-442, had a higher potency to neutralize the most antigenically distinct of the three viruses (SUDV) when compared, respectively, to the potency of EBOV-520 or EBOV-548. EBOV-515 monotherapy in mice also demonstrated a high level of therapeutic protection against SUDV (Gilchuk et al., 2018a, 2020b). Given the higher potency of EBOV-515 and EBOV-442 against SUDV, we suggest their combination as a candidate for a "next-generation" broad therapeutic mAb cocktail. In this study, we describe pre-clinical development of the EBOV-515 + EBOV-442 mAb cocktail and define the molecular basis for its pan-ebolavirus activity and efficacy.

RESULTS

Activities of pan-ebolavirus candidate cocktail containing recombinant mAbs rEBOV-442 and rEBOV-515

Antibody variable gene sequences for mAbs EBOV-515 and EBOV-442 were determined, and synthetic DNAs encoding the mAbs were used to produce recombinant IgG1. Recombinant (r) mAbs, designated as rEBOV-515 and rEBOV-442, potently neutralized EBOV, BDBV, and SUDV (Figure 1A) with a note that rEBOV-442 only partially neutralized SUDV (Gulu variant) but was more active against a chimeric vesicular stomatitis virus (VSV) expressing the Boniface variant of SUDV GP (see below). To assess the Fc-mediated effector function of these antibodies to mediate killing of antigen-expressing cells, we used a stably transfected EBOV GP-expressing SNAP-tagged 293F cell line as a target, with heterologous human peripheral blood mononuclear cells (PBMCs) as source of effector cells and a previously described assay (Domi et al., 2018). The glycan-cap-specific mAb rEBOV-442 immunoglobulin G1 (IgG1) exhibited a high level of cytotoxic activity, and the GP-base-specific mAb rEBOV-515 exhibited a moderate level of cytotoxic activity, relative to the control Fc-function-disabled IgG1-LALA-PG variant of rEBOV-515 (designated as rEBOV-515 LALA-PG) or an irrelevant mAb rDENV 2D22 (IgG1 isotype) specific to the dengue virus envelope (E) protein (Fibriansah et al., 2015) (Figure 1B). Neutralizing activity of the wild-type IgG1 and IgG1-LALA-PG variants of rEBOV-515 was equivalent (Figure S1A). These results taken together revealed two complementary activities exhibited by this broad mAb cocktail, specifically the Fc-mediated effector functions mediated by rEBOV-442 and the potent neutralizing activities mediated by rEBOV-442 and rEBOV-515 (Figure 1C).

One benefit of using a cocktail of two or more neutralizing mAbs that bind to non-overlapping regions of the viral antigen is to reduce the risk of viral escape from neutralization that is inherent in monotherapy approaches (Baum et al., 2020; Misasi and Sullivan, 2021; Yewdell et al., 1979). To demonstrate this feature for this cocktail directly, we next used a recombinant infectious VSV expressing EBOV or BDBV GP in place of the endogenous VSV glycoprotein (VSV/EBOV GP or VSV/BDBV GP) to select for GP mutations that escape mAb neutralization. We used rEBOV-442, rEBOV-515, or 1:1 mixture of both mAbs and a high-throughput quantitative real-time cellular analysis assay (RTCA) to select viral variants that can escape neutralization (Gilchuk et al., 2020b; Greaney et al., 2021). For comparative purposes, we also assessed the broadly reactive antibodies ADI-15878 and ADI-15946 that form the basis for a potent broadly protective investigational cocktail (Bornholdt et al., 2019; Wec et al., 2017). We used recombinant IgG1 proteins for these antibodies that we produced using publicly available mAb variable region sequences. ADI-15946, similarly to rEBOV-515, recognizes the loop region of the internal fusion loop (IFL), whereas ADI-15878 recognizes the stem region of the IFL (Gilchuk et al., 2018a; King et al., 2019) and, hence, the ADI-15878 binding site does not overlap with that of the other IFL-specific mAbs we tested. We selected for escape at a single saturating mAb concentration of 20 μg/mL using ~1 multiplicity of infection (MOI) and performing 60–154 replicates for each sample (Figure S1B). Only one to two passages with individual mAbs

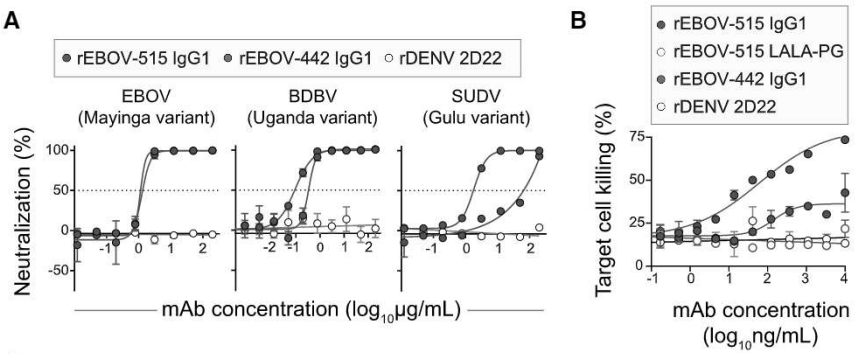

C

mAb	GP binding by ELISA (EC_{50}; ng/mL)					Virus neutralization (IC_{50}; ng/mL)			Fc region - mediated cytotoxicity (relative)	Site on GP*	% protection in mice (EBOV)*
	EBOV	BDBV	SUDV	MARV	EBOV sGP	EBOV	BDBV	SUDV			
rEBOV-442 IgG1	9	20	61	>	2	1,241	899	~64,000	High	Glycan cap	80-100
rEBOV-515 IgG1	47	91	263	>	>	1,117	339	1,808	Low	Base	100

D

Antibody	Virus for escape selection	Replicates with escape / total replicates (%)	Confirmed escape at 20 µg/mL mAb	Escape from neutralization by indicated mAb (Yes/No)	Mutations selected (X number of times/ of Y sequenced escapes)
rEBOV-442	VSV/EBOV GP	60/60 (100%)	Yes (all tested)	**rEBOV-442 (Yes)** rEBOV-515 (No) Cocktail (No) ADI-15878 (No) ADI-15946 (No)	L273P (7/7)**; F234V (2/7); G271E (1/7); K272Q (1/7); I274V (1/7); K280E (1/7); V311A (2/7)
rEBOV-515		0/154 (0%)	Not applicable	Not applicable	Not applicable
Cocktail (1:1)		0/60 (0%)	Not applicable	Not applicable	Not applicable
ADI-15878		6/94 (6%)	Yes (all tested)	rEBOV-442 (No) rEBOV-515 (No) **ADI-15878 (Yes)** ADI-15946 (No)	Q560K (1/3); Q560R (2/3)
ADI-15946		24/94 (25%)	Yes (all tested)	rEBOV-442 (No) rEBOV-515 (No) ADI-15878 (No) **ADI-15946 (Yes)**	G74R (2/2)
rEBOV-515	VSV/BDBV GP	0/94 (0%)	Not applicable	Not applicable	Not applicable
ADI-15878		94/94 (100%)	Yes (all tested)	rEBOV-442 (No) rEBOV-515 (No) **ADI-15878 (Yes)** ADI-15946 (No)	R130K (3/3); G528S (3/3)
ADI-15946		14/94 (15%)	Yes (all tested)	rEBOV-442 (No) rEBOV-515 (No) ADI-5878 (No) **ADI-15946 (Yes)**	N514Y (1/3); I542T (3/3); N556D (1/3); ([K510E, Δ292-477] (1/3))

Figure 1. Functional activities of pan-ebolavirus cocktail candidate mAbs rEBOV-442 and rEBOV-515

(A) EBOV, BDBV, or SUDV neutralization. Ebolaviruses encoding enhanced green fluorescent protein (eGFP) were incubated with increasing concentrations of recombinantly produced purified mAbs, and infection was determined at 3 days after inoculation by measuring eGFP fluorescence in cells. Mean ± SD of technical triplicates from one experiment are shown.

(B) *In vitro* killing capacity mediated by the Fc regions of IgG1-engineered variants of mAbs measured by rapid fluorometric antibody-mediated cytotoxicity (RFADCC) assay. Human PBMCs (effector cells) were incubated with a SNAP-tagged EBOV GP-expressing 293F cell line as a target in the presence of increasing concentrations of purified recombinant mAbs, and cytotoxic activity was measured by flow cytometry. Antibody rDENV 2D22 served as a negative control. The dotted line indicates assay background. Mean ± SD of technical duplicates from one experiment are shown.

(C) Heatmap summarizing reactivity breadth and potency of rEBOV-442 and rEBOV-515. *Indicates data determined in our previous work using hybridoma-cell-secreted mAbs (Gilchuk et al., 2018a).

(D) Results of viral selections with individual antibodies or the combination of rEBOV-442 + rEBOV-515 (defined as the "cocktail"), indicating the number of replicates with escape out of total number tested, resistance of selected escape variants to individual antibodies or the cocktail, and the selected mutations in the GP that escape neutralization by indicated mAb. Broadly neutralizing mAbs ADI-15878 and ADI-15946 (Wec et al., 2017) were included for comparative purposes. The escape selection was performed using chimeric VSV expressing EBOV or BDBV GP.

See also Figure S1.

rEBOV-442, ADI-15878, or ADI-15946 led to selection of variants resistant to neutralization by 20 µg/mL of mAb used for the escape selection. For rEBOV-515 or the rEBOV-442 + rEBOV-515 cocktail, escape variants were not detected in any of the 154 or 60 replicate experiments and after two passages (Figure 1D), suggesting a lower likelihood of *in vitro* escape for rEBOV-515 or the cocktail. Viruses that escaped neutralization by rEBOV-442 were fully neutralized by rEBOV-515 or a mixture of rEBOV-442 and rEBOV-515 (Figures 1D and S1C), showing that the cocktail retains neutralization potency even if rEBOV-442 is impacted. Importantly, the viruses selected to be resistant to neutralization by each single mAb rEBOV-442, ADI-15878, or ADI-15946 were sensitive to neutralization by each of three other mAbs, highlighting the differences for these mAbs in their binding site residues (Figures 1D and S1C). We sequenced the viral gene encoding the GP of selected escape viruses and identified distinct point mutations (Figure 1D), including several previously identified escape mutations at amino acid positions L273 for rEBOV-442 (Gilchuk et al., 2018a), K510 for ADI-15946, and G528 for ADI-15878 (Wec et al., 2017). In all cases, escape viruses carried GP mutations in the binding site of the respective mAb (Figure S1D). Together, these results demonstrated a high resistance to viral escape for the cocktail of the rEBOV-442 + rEBOV-515, which acts by both neutralizing and Fc-mediated activities.

Differential requirements for the Fc regions of antibodies rEBOV-442 and rEBOV-515 for therapeutic protection in mice

To define the contribution of Fc-mediated effector functions to protection *in vivo*, each mAb of the candidate therapeutic cocktail was assessed as an IgG1 protein (the original subclass of mAb secreted by the hybridoma cell line and a functionally competent form of mAb) and as an IgG1 LALA-PG protein that is disabled

for Fc function. The Fc region of the LALA-PG variant has three mutations, L234A, L235A, and P329G, which eliminate complement binding and Fc-γ-receptor-dependent, antibody-dependent, cell-mediated cytotoxicity in both murine IgG2a and human IgG1 (Lo et al., 2017). We challenged groups of mice with mouse-adapted EBOV (EBOV-MA) on day 0 and administered mAbs 1 day later. We chose different treatment doses of rEBOV-515 (1 mg/kg) and rEBOV-442 (5 mg/kg) based on the known *in vivo* potency of the parental hybridoma-produced mAbs EBOV-442 (moderate potency at 5 mg/kg) and EBOV-515 (high potency at 5 mg/kg) (Gilchuk et al., 2018a). Previously we have shown that for low-dose treatment (1 mg/kg), the Fc-disabled LALA variant of the GP base-specific mAb EBOV-520 (that is analogous to rEBOV-515 based on competition binding) offered a higher level of therapeutic protection in mice against EBOV (60% survival) when compared to that mediated by the wild-type (WT) IgG1 EBOV-520 (0% survival) (Kuzmina et al., 2018). Given the full protection from weight loss and disease conferred by the 5 mg/kg dose of hybridoma-expressed EBOV-515 (Gilchuk et al., 2018a), and to compare with the reported potency for low-dose EBOV-520 treatment, in this study, we tested the recombinant variants of rEBOV-515 using a 1 mg/kg low-dose treatment. For comparative purposes, we also assessed the broadly reactive mAbs ADI-15946 (1 mg/kg; analogous to rEBOV-515) and ADI-15878 (5 mg/kg; recognizing a distinct epitope on IFL) (Wec et al., 2017) as IgG1 proteins. The rEBOV-515 LALA-PG variant offered complete protection (100% survival) against EBOV challenge in mice at a 1 mg/kg therapeutic dose, whereas the WT IgG1 variant showed partial protection (80% survival) (Figure 2). ADI-15946 IgG1 did not protect at 1 mg/kg. This finding demonstrated a higher *in vivo* potency of the broad GP base-specific mAb rEBOV-515 when compared to the previously reported effect of the broad GP base-specific mAb rEBOV-520 or ADI-15946 IgG1, and suggested that rEBOV-515 LALA-PG is a preferable Fc variant for the cocktail of two Fc variants tested.

Similarly, we compared the *in vivo* potency of WT IgG1 rEBOV-442 and rEBOV-442 LALA-PG, which were administered at a 5 mg/kg dose 1 day after EBOV challenge (Figure 2). Cytotoxicity assay results (Figure 1B) suggested that the glycan cap mAb rEBOV-442, in addition to possessing neutralizing activity, also exhibited substantial Fc effector function-mediated activity. In agreement with this finding, the results of our *in vivo* study showed a transient improvement in weight (i.e., reduced loss) on 2–4 and 8–10 days post-infection with WT rEBOV-442 IgG1, which was associated with improved protection from death (90% survival in the WT mAb-treated group when compared to 70% in the rEBOV-442 LALA-PG-treated group) and faster recovery from illness (Figure 2). ADI-15878 IgG1 at 5 mg/kg fully protected mice against EBOV. Together, these data revealed differing requirements for the Fc regions of rEBOV-442 and rEBOV-515, demonstrated a high *in vivo* potency of the mAbs tested, and justified the inclusion of rEBOV-515 as a LALA-PG and rEBOV-442 as a WT IgG1 in a new broad and protective ebolavirus two-antibody cocktail.

Synergistic activity of rEBOV-442 and rEBOV-515 in the cocktail

Antibodies in a cocktail directed to a common viral protein may recognize antigen in a synergistic, additive, or antagonistic manner. We first characterized the effect mediated by the mixture of two mAbs on ebolavirus GP binding. Serially diluted Alexa Fluor-647-labeled mAb rEBOV-442 IgG1 or rEBOV-515 LALA-PG was titrated into serially diluted unlabeled partner mAb to generate two pairwise combinatorial matrices of two mAbs in the mixture (Figures S2A and S2B). Binding of the Alexa Fluor-647-labeled mAb from each combination was assessed by flow cytometric analysis using a Jurkat cell line that was stably transduced to display EBOV GP on the surface as described before (Gilchuk et al., 2020b). The values were calculated as the percent of the relative fluorescence signal caused by the highest concentration of respective fluorescently labeled mAb alone (Figures S2A and S2B), and then compared with the expected responses calculated using the ZIP synergy-scoring model (Ianevski et al., 2020). The synergy score can be interpreted as the average excess response (percent change) for the mAb combination (Ianevski et al., 2020). The comparison revealed that the combination of mAbs rEBOV-442 and rEBOV-515 was synergistic, and each mAb reciprocally enhanced binding of the partner mAb in the mixture (Figures S2B and S2C). This finding contrasted with the unidirectional GP binding synergy observed in the cocktail of the other broad mAbs rEBOV-520 and rEBOV-548 (Gilchuk et al., 2020b). Binding enhancement increased steadily with increasing of mAb concentration, indicating more contribution from synergy at higher concentrations of individual mAbs in the cocktail (Figures S2B and S2C).

We next characterized the effect by the mixture of two mAbs on ebolavirus neutralization. Using a recently developed RTCA assay and infectious chimeric VSV/ebolavirus GP viruses (Gilchuk et al., 2020a, 2020b), we showed dose-dependent neutralization of VSV/EBOV GP, VSV/BDBV GP, or VSV/SUDV GP viruses by the 1:1 mAb mixture (Figure 3A). Then, we titrated serially diluted rEBOV-442 into serially diluted rEBOV-515 to generate a pairwise combinatorial matrix of two mAbs in the mixture and assessed each combination for neutralization of VSV/EBOV GP, VSV/BDBV GP, or VSV/SUDV GP viruses (Figure 3B). Synergy analysis identified areas in the neutralization matrix (showing mAb ratios) with the most profound combination effect and suggested broad synergistic activity in the cocktail of rEBOV-442 and rEBOV-515 (Figure 3C). Synergistic activity mediated by the cocktail also was confirmed using neutralization assays with authentic live ebolaviruses, and more prominent synergy of neutralization was identified for SUDV (Figure S3).

Protective pan-ebolavirus combination therapy of nonhuman primates by antibodies rEBOV-442 and rEBOV-515

Next, we tested the efficacy of the cocktail of rEBOV-515 LALA-PG + rEBOV-442 IgG1 in nonhuman primate (NHP) challenge models for each of the three ebolaviruses, EBOV (Kikwit variant), BDBV (Uganda variant), and SUDV (Gulu variant). We chose a 2:1 mAb ratio in the cocktail (66.5% rEBOV-515 LALA-PG and 33.5% rEBOV-442 IgG1 in the mixture) empirically. We biased the composition using a higher proportion of rEBOV-515 LALA-PG based on several principles: (1) higher neutralizing potency of rEBOV-515 against SUDV, (2) higher protective efficacy of rEBOV-515 *in vivo*, and (3) higher resistance against mutational

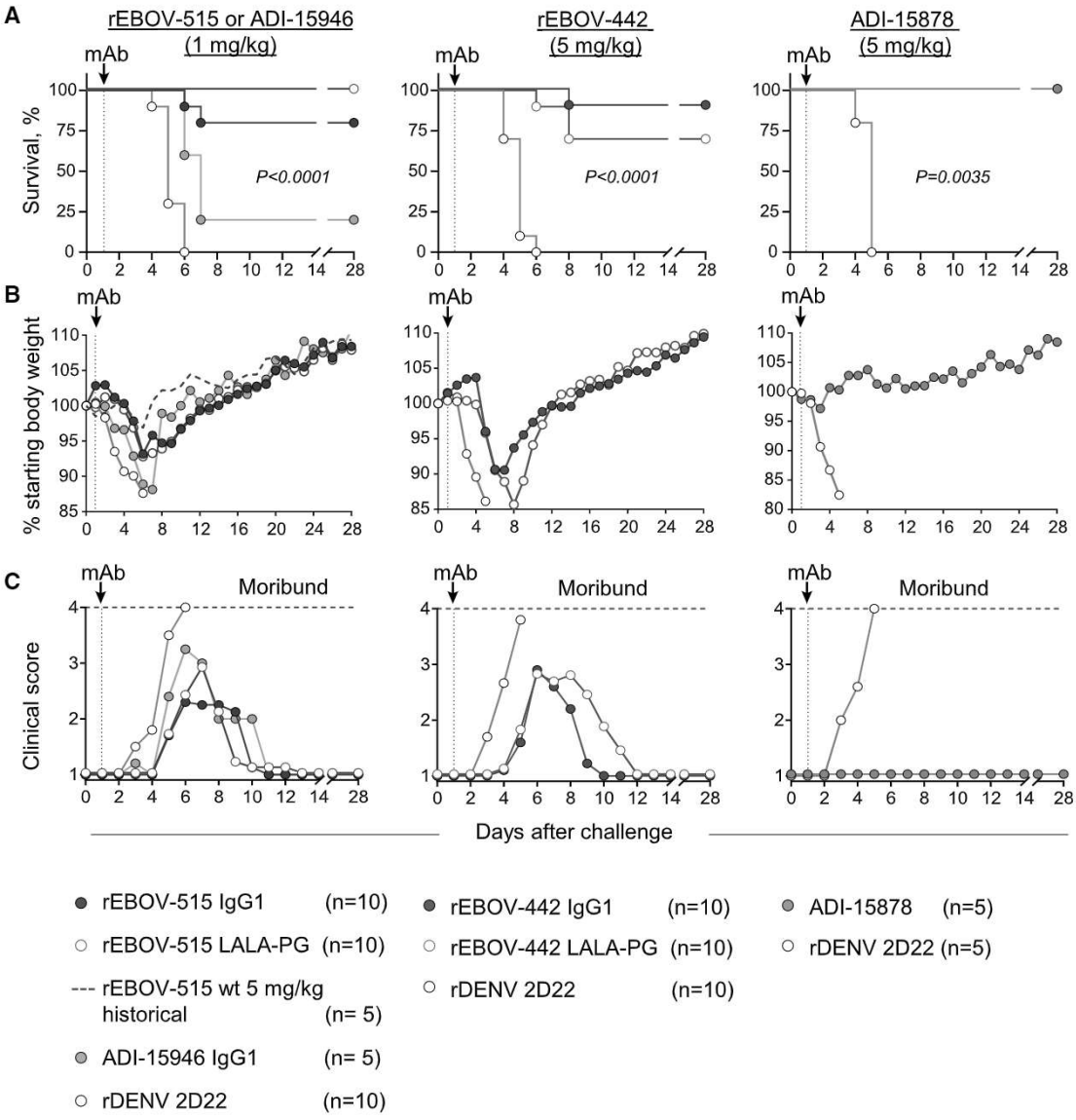

Figure 2. Differential requirements for the Fc regions of mAbs rEBOV-442 and rEBOV-515 for optimal therapeutic protection in mice

C57BL/6 mice were challenged with EBOV-MA (day 0), treated at 1 day post infection (dpi) with wild-type IgG1 or IgG1 LALA-PG variant of mAbs rEBOV-442 (5 mg/kg) and rEBOV-515 (1 mg/kg), and monitored for 28 days. Antibodies ADI-15946 IgG1 (1 mg/kg) and ADI-15878 IgG1 (5 mg/kg) were included for comparative purposes, and mAb rDENV 2D22 was used as a control.

(A) Kaplan-Meier survival plot. The overall difference in survival between the groups was estimated using two-sided log-rank (Mantel-Cox) test.

(B) Weight change. A historical control for protection from weight loss with 5 mg/kg of hybridoma-produced mAb EBOV-515 treatment (Gilchuk et al., 2018a) is indicated with a raspberry dotted line.

(C) Clinical score.

Mean values are shown in (B) and (C). For the rEBOV-515 and rEBOV-442 treatment groups, a total of n = 10 mice per group was analyzed in two independent experiments for which cumulative data are shown. For the ADI-15946 and ADI-15878 treatment groups, data represent one experiment with 5 mice per group. Body-weight-change and clinical score data in (B) and (C) are shown only for the animals that survived at each indicated time point. Time points for mAb treatment are indicated with dotted vertical lines

escape in the presence of rEBOV-515 *in vitro* when compared to that of rEBOV-442. Of note, at this ratio, the mAbs exhibited synergy in the cocktail to neutralize the virus as determined from the synergy distribution maps (Figures 3 and S3). We used rhesus macaque EBOV and SUDV lethal challenge models and a cynomolgus monkey BDBV lethal challenge model, which recapitulate many key features of EVD in humans (Bennett et al., 2017; Geisbert et al., 2015). Animals were assigned to three treatment groups of five animals per group. After intramuscular challenge with a lethal target dose of 1,000 plaque-forming units (PFUs) of EBOV, BDBV, or SUDV, all NHPs of the treatment group received intravenously two 30 mg/kg doses of the cocktail

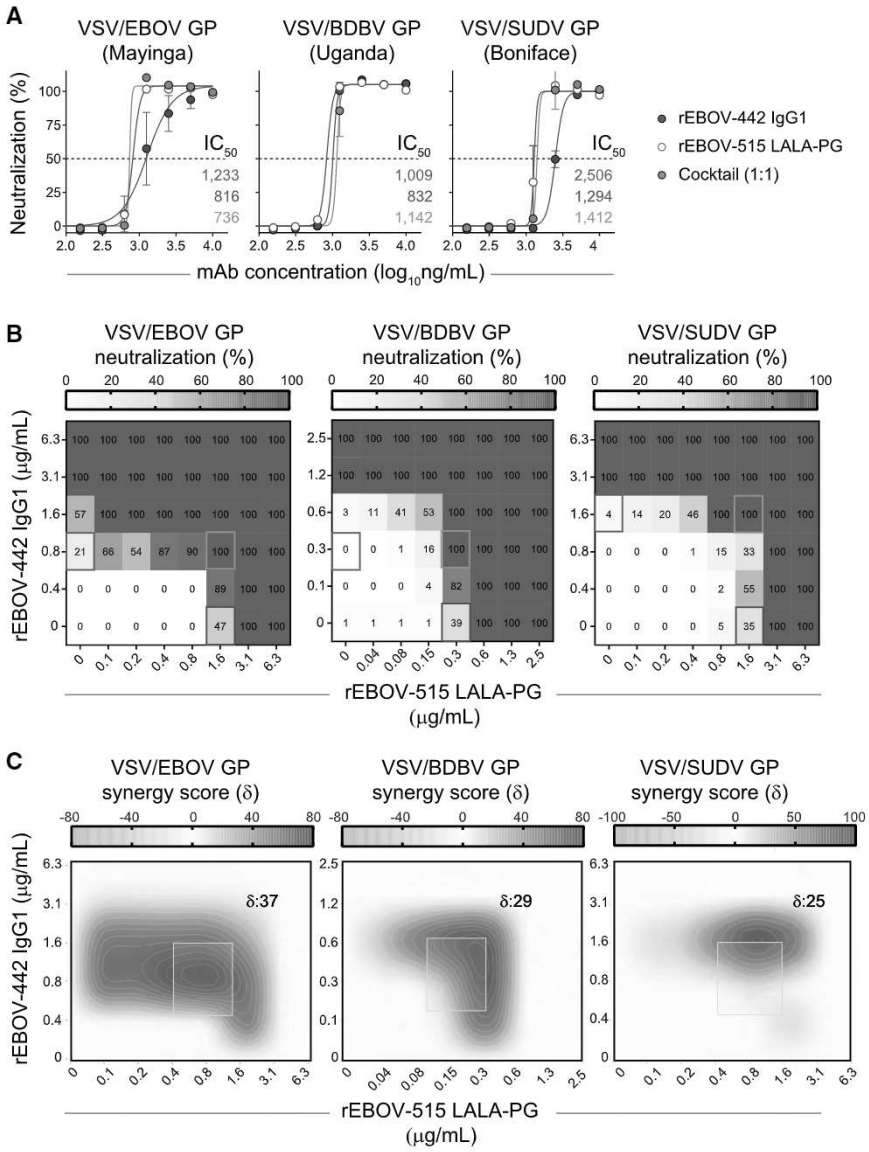

Figure 3. Broad and synergistic neutralizing activity mediated by the cocktail of rEBOV-442 and rEBOV-515

Neutralizing activity of individual mAbs or their mixture was assessed using chimeric VSV viruses and RTCA assay.

(A) Neutralization of VSV/EBOV GP, VSV/BDBV GP, or VSV/SUDV GP by rEBOV-442 alone, rEBOV-515 alone, or a 1:1 mixture of rEBOV-442 and rEBOV-515. Mean ± SD of technical duplicates is shown.

(B) Serially diluted rEBOV-442 was titrated into serially diluted rEBOV-515 to generate a pairwise combinatorial matrix of two mAbs in the mixture. The matrix shows neutralization dose-response data for VSV/EBOV GP, VSV/BDBV GP, or VSV/SUDV GP, by indicated concentrations of rEBOV-442 and rEBOV-515. Axes denote the concentration of each mAb, with the percent neutralization shown in each square. The heatmap denotes a gradient of 0 (white) to 100% (red) neutralization. Examples of neutralization by rEBOV-515 alone (raspberry box) or rEBOV-442 alone (blue box) in comparison to a combined indicated concentration of two mAbs in the cocktail (green box) is shown.

(C) Synergy distribution map generated from the dose-response neutralization matrix in (B). Red color indicates areas in which synergistic neutralization was observed; shaded gray box indicates the area of maximum synergy between the two mAbs, and the δ-score for this area is shown. The δ-score is a synergy score: values <−10 indicate antagonism; values −10 to 10 indicate an additive effect; values >10 indicate synergy. Data in (A)–(C) are from a representative experiment performed in technical duplicate and repeated three times.

See also Figures S2 and S3.

spaced 3 days apart (given days 3 and 6 after EBOV, days 6 and 9 after BDBV, or days 4 and 7 after SUDV inoculation). For each challenge cohort, an additional animal was studied as a contemporaneous control and was left untreated. The untreated control animals developed a high clinical score and succumbed to disease on day 6, 14, or 10 after viral challenge with EBOV, BDBV, or SUDV, respectively. The two-dose therapeutic cocktail treatment provided complete pan-ebolavirus protection of NHPs from mortality and clinical signs of EVD (Figures 4A and 4B). We next assessed changes in blood chemistries and blood cell composition that are typically associated with EVD to further characterize the efficacy of the mAb treatment (Tables S1, S2, S3, S4, S5, and S6). The liver enzymes alkaline phosphatase (ALP) and gamma glutamyl transferase (GGT), which are indicators of EVD (Qiu et al., 2014), were elevated in untreated NHPs at the peak of the disease (Figure 4C). Treated animals did not show signs of acute liver injury after the treatment, displaying low amounts of ALP, GGT, creatinine (CRE), and the other blood chemistries when compared with those of untreated NHP (Figure 4C; Tables S4, S5, and S6).

At the time of first treatment with the cocktail (day 3 after EBOV, day 6 after BDBV, or day 4 after SUDV inoculation), 14 NHPs from the treatment-designated group (all except one animal in EBOV-challenged group) and the control untreated NHPs were viremic and non-symptomatic, with virus titers that ranged from 5.1 to 10.6 $\log_{10}$ genome equivalents (GEQs) per mL of plasma, as measured by quantitative reverse-transcription PCR (qRT-PCR) (Figure 5A). A plaque assay that detects infectious virus revealed viremia in all 18 animals, with viral titers ranging from 0.7 to 7.4 $\log_{10}$ PFUs per mL of plasma at the time of first treatment with the cocktail (Figure 5B). This finding confirmed active ebolavirus infection in all NHPs before treatment. At the time of the second mAb treatment (day 6 after EBOV, days 9 after BDBV, or day 7 after SUDV inoculation), each untreated control NHP from a respective EBOV, BDBV, or SUDV challenge cohort developed high viremia >8 $\log_{10}$ GEQ/mL and >5 $\log_{10}$ PFU/mL (Figures 5A and 5B). Concordant with full protection from disease and

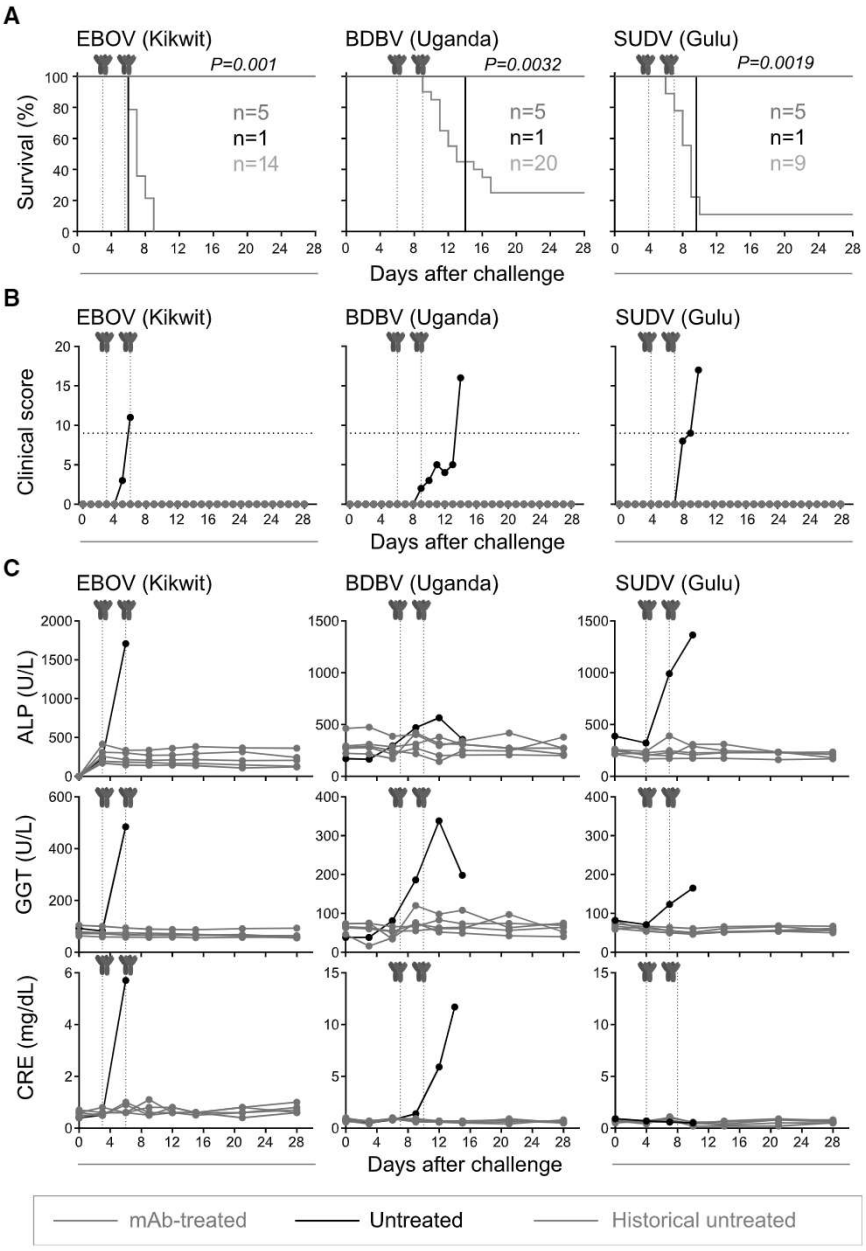

Figure 4. The cocktail treatment provides pan-ebolavirus protection of nonhuman primates against disease

Rhesus macaques were inoculated with a lethal dose of the EBOV/Kikwit or SUDV/Gulu viruses intramuscularly (i.m.) on day 0 and were treated with total 30 mg/kg of the cocktail (1:2 mixture of rEBOV-442 and rEBOV-515) intravenously on 3 and 6 dpi (EBOV/Kikwit; n = 5 per cohort), or 4 and 7 dpi (SUDV/Gulu; n = 5 per cohort). Cynomolgus monkeys were inoculated with a lethal dose of the BDBV/Uganda i.m. on day 0 and were treated with a total dose of 30 mg/kg of the cocktail (1:2 mixture of rEBOV-442 and rEBOV-515) intravenously on 6 and 9 dpi (n = 5 per cohort). The contemporaneous control was an untreated NHP challenged with the virus (n = 1 for each cohort). One experiment was performed.

(A) Kaplan-Meier survival plot. The historical untreated controls (gray) are shown for comparative purposes (see STAR Methods). The proportion surviving at day 28 after viral challenge in the treated cohort was compared to the respective historical untreated cohort using a 2-sided exact unconditional test of homogeneity.

(B) Clinical score.

(C) Selected blood chemistry measurements: ALP, alkaline phosphatase; GGT, gamma-glutamyl transpeptidase; CRE, creatinine. Antibody treatment times are indicated with blue dotted vertical lines. Orange curves indicate treated, and black indicate untreated animals in (A)–(C). The black dotted line in (B) indicates the clinical score threshold for euthanasia.

Time points for mAb treatment are indicated with dotted vertical lines in (A)–(C).

See also Tables S1, S2, S3, S4, S5, and S6.

death, none of the 15 treated NHPs had detectable infectious virus in the plasma at that time (limit of detection [LOD] = 5 PFU/mL), and viral genomes were not detected in 12 of those NHPs 3.7 (LOD = $\log_{10}$ GEQ/mL) at that time (Figures 4 and 5). The three remaining NHPs that were from the BDBV inoculation cohort and that showed slightly delayed clearance of viral genomes in plasma no longer had detectable virus by day 15 after viral challenge. Analysis of various tissues harvested at study endpoint from treated animals (day 28 after inoculation with EBOV and SUDV or day 35 after inoculation with BDBV) and untreated animals (day 6, 14, or 10 after inoculation with EBOV, BDBV, or SUDV, respectively) revealed varying levels of viral RNA as a sign of systemic infection that had been established before the treatment (Figure 5C). It has been shown previously that in the case of treatment failure, the infectious virus can be readily detected by plaque assay (Oswald et al., 2007). Therefore, we next assessed the infectious virus load in 11 representative immune-privileged tissues of treated NHPs from each cohort that was selected based on the highest viral RNA load. Infectious virus was not detected in any of these tissues (Figure 5D), confirming virologic protection mediated by the cocktail treatment.

Together, these results showed a high therapeutic efficacy of the cocktail of rEBOV-515 LALA-PG + rEBOV-442 IgG1 to treat established viremia, clear the infectious virus from immune-privileged tissues, and prevent disease caused by EBOV, BDBV, and SUDV.

Structural basis for the efficacy and broad ebolavirus neutralization by the cocktail

We previously reported the molecular determinants of the GP binding for several glycan cap-specific mAbs, including the

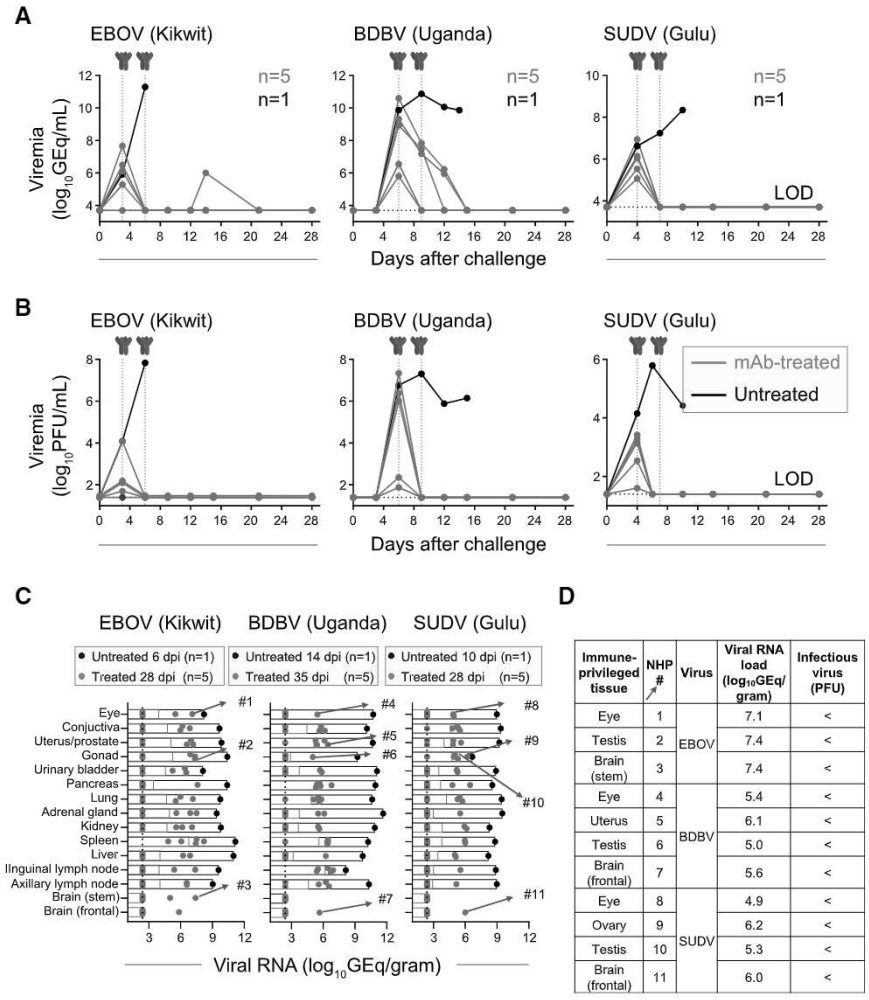

D

Immune-privileged tissue	NHP #	Virus	Viral RNA load (log_{10}GEq/gram)	Infectious virus (PFU)
Eye	1	EBOV	7.1	<
Testis	2		7.4	<
Brain (stem)	3		7.4	<
Eye	4	BDBV	5.4	<
Uterus	5		6.1	<
Testis	6		5.0	<
Brain (frontal)	7		5.6	<
Eye	8	SUDV	4.9	<
Ovary	9		6.2	<
Testis	10		5.3	<
Brain (frontal)	11		6.0	<

Figure 5. The cocktail treatment provides pan-ebolavirus protection of nonhuman primates against viremia

Blood viral loads were assessed from individual animals that were challenged with EBOV/Kikwit, BDBV/Uganda, or SUDV/Gulu and treated with the two-antibody cocktail as described in Figure 4.

(A) Kinetics of blood viral load determined for genome equivalents (GEq) using qRT-PCR.

(B) Kinetics of infectious virus blood viral load as determined by plaque assay. Orange curves indicate treated, and black indicate untreated animals. Antibody treatment times are indicated with blue dotted vertical lines. The black dotted line indicates the limit of detection (LOD), which was 3.7 log_{10}GEq/mL (A) or 25 PFU/mL (B). Violet dot indicates one NHP confirmed to be viremic (5 PFU/mL; LOD = 2 PFU/mL) at 3 dpi upon repeated test using a lower plasma dilution.

(C) Viral RNA load in various peripheral tissues of treated NHPs (28 dpi for EBOV and SUDV cohort or 35 dpi for BDBV cohort). Tissues from succumbed untreated NHP from each cohort were used as controls. The black dotted vertical line indicates the limit of detection, which was 2.4 log_{10}GEq/gram. The data are shown as an aligned dot plot with bar, where orange dots indicate measurement from individual treated animals, black dots and bars indicate measurement from untreated control animals, and orange bar indicates the mean value of the measurements for treated cohorts. For samples in which viral RNA was not detected, the measurement values were set to the limit of detection, 2.4 log_{10}GEq/gram. Brain samples from untreated animals have not been tested. Arrows with numbers indicate immune privileged tissues selected for assessment of infectious virus load as in (D).

(D) Plaque assay measurements of infectious virus load in representative immune privileged tissues of treated NHPs from each cohort that were selected based on the highest viral RNA load as in (C). The < symbol indicates infections virus was not detected, and the LOD was 250 PFU/gram of tissue.

Each measurement in (A)–(D) represents the mean of technical duplicates. The dotted vertical lines in (A) and (B) indicate time points for mAb treatment.

broad mAb rEBOV-442 (Murin et al., 2021), and defined the structural basis of synergy for the pair of broad mAbs rEBOV-520 and rEBOV-548 (Gilchuk et al., 2020b). In this new study, we focused on studies of the determinants of rEBOV-515 binding to elucidate the structural basis for the neutralization breadth and efficacy mediated by pan-ebolavirus cocktail of rEBOV-515 + rEBOV-442. We generated a complex of both rEBOV-515 and rEBOV-442 Fab with mucin-like domain-deleted EBOV GP from the Makona variant (EBOV GPΔMuc/Mak) and solved structures by cryogenic electron microscopy (cryo-EM) (Figures 6A and S4; Table S7).

The interface between GP and rEBOV-515 in this structure was resolved to ~3 to 3.5 Å resolution (Figure S4), allowing for confident modeling of most of the side-chain residues. rEBOV-515 binds to the base of the IFL, directly below the glycan cap in GP1 (Figure 6A). There is significant overlap of the rEBOV-515 epitope with that of rEBOV-520, but rEBOV-515 has more extensive contacts in GP2 and less in GP1 (Figure 6B). Most EBOV-515 contacts are mediated by the heavy chain (HC), with all three complementarity determining regions (CDRs) contributing to binding the base of the IFL as well as a portion of GP1 near the 3_{10} pocket (Figures 6C, S5A, S5B, and S6). The CDRH3 contributes the most extensive contacts, including those that displace the descending β17-β18 loop of the glycan cap, making contacts near the 3_{10} pocket, as well as a strong cation-pi bond with $R136_{GP1}$ (Figure 6C). The rEBOV-515 light chain (LC) also makes contacts with all three CDRs exclusively within GP2 (Figures 6D and S5A). Together, this analysis showed that rEBOV-515 forms a strong interaction of complementary hydrophobic (Figure S5B) and electrostatic (Figure S5C) surfaces for binding to this epitope within GP.

Neutralizing potency may depend on the ability of mAb to remain bound to viral GP within the acidic environment of late endosomes, which is where pH-dependent cleavage occurs to expose the Niemann-Pick C1 (NPC1) receptor binding site (Carette et al., 2011; Chandran et al., 2005). Given that rEBOV-515 strongly interacts with the EBOV GP, we assessed binding of this mAb at varying pH to recombinant EBOV, BDBV, or

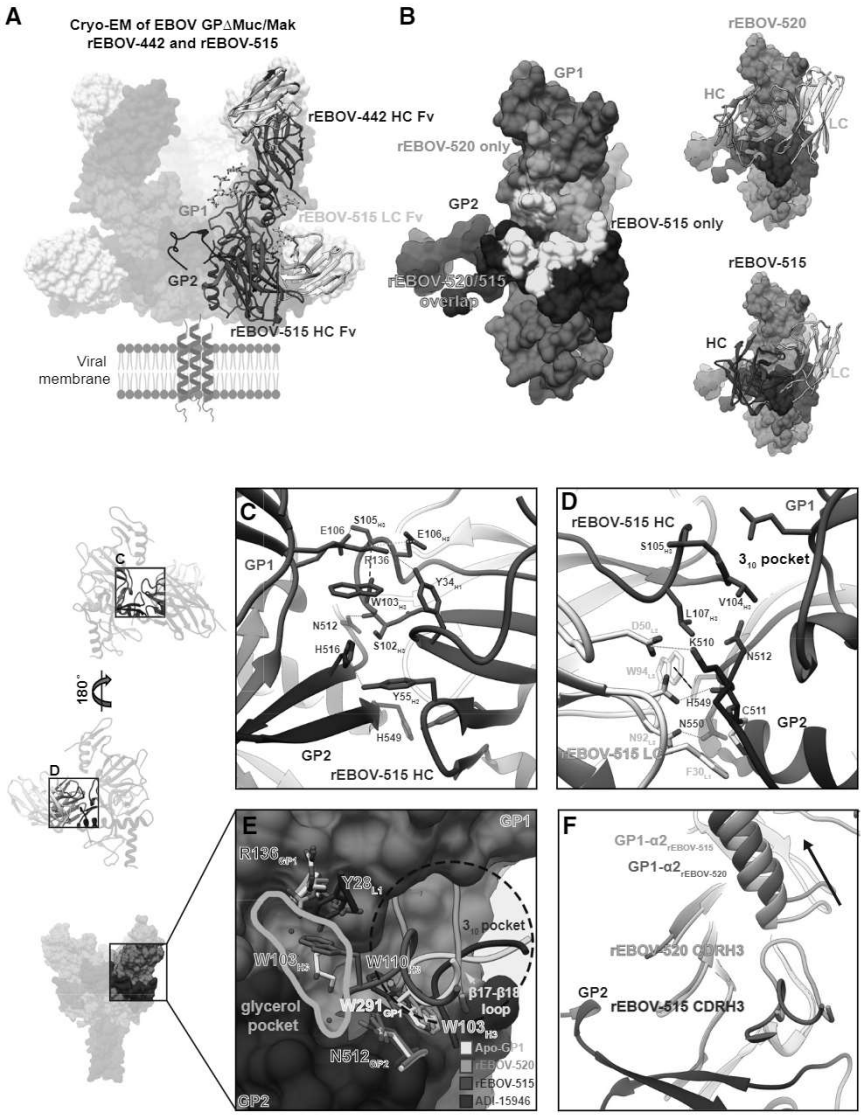

Figure 6. rEBOV-515 binds to the major site of vulnerability in the GP base region in a distinct manner

(A) Cryo-EM structure of rEBOV-442 (heavy chain in blue and light chain in gray) and rEBOV-515 (heavy chain in maroon and light chain in pink) Fab bound to EBOV GPΔMuc/Mak. A side view in relation to the viral membrane is shown. Fab constant domains were excluded by masking.

(B) The predicted contact surface of broadly neutralizing mAbs rEBOV-515 and rEBOV-520 on the surface representation of the EBOV GPΔMuc/Mak monomer model (PDB: 5JQ3). Non-overlapping contact surfaces for rEBOV-515 or rEBOV-520 are shown, respectively, in maroon or orange, and overlapping contact surface of both mAbs is shown in yellow.

(C) Contact residue details of the rEBOV-515 heavy chain Fab interactions with the base of GP. CDRH3 contacts include a backbone-mediated hydrogen bond at $S102_{H3}$ to $N512_{GP2}$, a key contact that links the β17-β18 loop to the base of the IFL via W291 in unliganded GP1. Contacts near the 3_{10} pocket include a potential hydrogen bond between $S105_{H3}$ and $E106_{GP1}$ that forms when a large portion of the CDRH3 loop displaces the β17-β18 loop. Within the CDRH2 loop, $Y52_{H2}$ and $Y55_{H2}$ make potential hydrogen bonds via their hydroxyl groups to $H549_{GP2}$ or $H516_{GP2}$ on GP2, respectively. One of the most extensive rEBOV-515 contacts is from $W103_{H3}$, which forms a strong cation-pi bond with $R136_{GP1}$, allowing R136 to make additional hydrogen bonds with $Y34_{H1}$ and a salt bridge with $E106_{H3}$.

(D) Epitope details of the rEBOV-515 light chain interactions with the base of GP. The rEBOV-515 light chain makes contacts with all three CDRs exclusively within GP2. Contact features include a potential hydrogen bond between $N32_{L1}$ and the backbone of $C511_{GP2}$, and a salt bridge between $D50_{L2}$ and $K510_{GP2}$. Pi cation interactions at $W94_{L3}$ with $H549_{GP2}$ (black dashed line) and an additional potential hydrogen bond at $N92_{L3}$ with $N550_{GP2}$ provide additional stabilizing interactions.

(E) Comparison of mAb CDRH3 loops that bind in and around the 3_{10} pocket (blue dashed circle) and putative glycerol pocket (solid yellow line). rEBOV-520 and ADI-15946 replace and mimic residue $W291_{GP1}$ (that anchors down the β17-β18 loop in apo-GP) with a tryptophan from their CDRH3 loops. rEBOV-515 uses an analogous tryptophan residue ($W103_{H3}$) to contact $R136_{GP1}$ via a strong cation-pi interactions bond, which causes a shift in the rotamer of $R136_{GP1}$. $W103_{H3}$ from rEBOV-515 also accesses a pocket that is occupied by a glycerol cryoprotectant molecule in the unliganded crystal structure of GP, which is also occupied by $Y28_{L1}$ from ADI-15946.

(F) A shift in the placement of the GP1 α2 helix that cased by the CDRH3 from rEBOV-520 but is lacking in rEBOV-515 binding due to a shorter CDR loop is shown. In (C) and (D): red dotted lines, hydrogen bonds; green dotted lines, salt bridge; purple dashed line, cation-pi interaction; black dashed line, carbon-pi or aromatic interactions. rEBOV-520-GP, PDB: 6PCI; ADI-15946-GP, PDB: 6MAM.

See also Figures S4, S5, and S6 and Table S7.

SUDV GPs. We used the broadly reactive base-specific mAb rEBOV-520 for comparison. rEBOV-515 and rEBOV-520 bound equivalently to the GP of each of the three ebolaviruses at neutral pH 7.4, and rEBOV-515 remained bound at acidic pH of 5.5 or 4.5, whereas rEBOV-520 lost binding activity (Figure S7A).

The rEBOV-515 binding site partially overlaps with those of other reported broad mAbs that bind to the 3_{10} pocket, including rEBOV-520 (Gilchuk et al., 2020b) and ADI-15946 (West et al., 2019) (Figures 6B and 6E). Each of these mAbs relies upon E106 and R136 in GP1 and several residues at the base of the IFL, using long CDRH3 loops that mimic and replace the β17-β18 loop of the GP1 in apo-GP structure (Figure 6E). However, characterization of the rEBOV-515 binding site revealed several unique features. rEBOV-515 uses a single CDR loop to simultaneously mimic and displace the β17-β18 loop and to bind to R136 in GP1. This feature allows rEBOV-515 to access a region that is occupied by a glycerol cryoprotectant molecule in the unliganded crystal structure of GP (PDB: 5JQ3 and 5JQB) that we defined as "glycerol pocket" (Figure 6E). In addition, this mechanism facilitates greater interaction of EBOV-515 with the

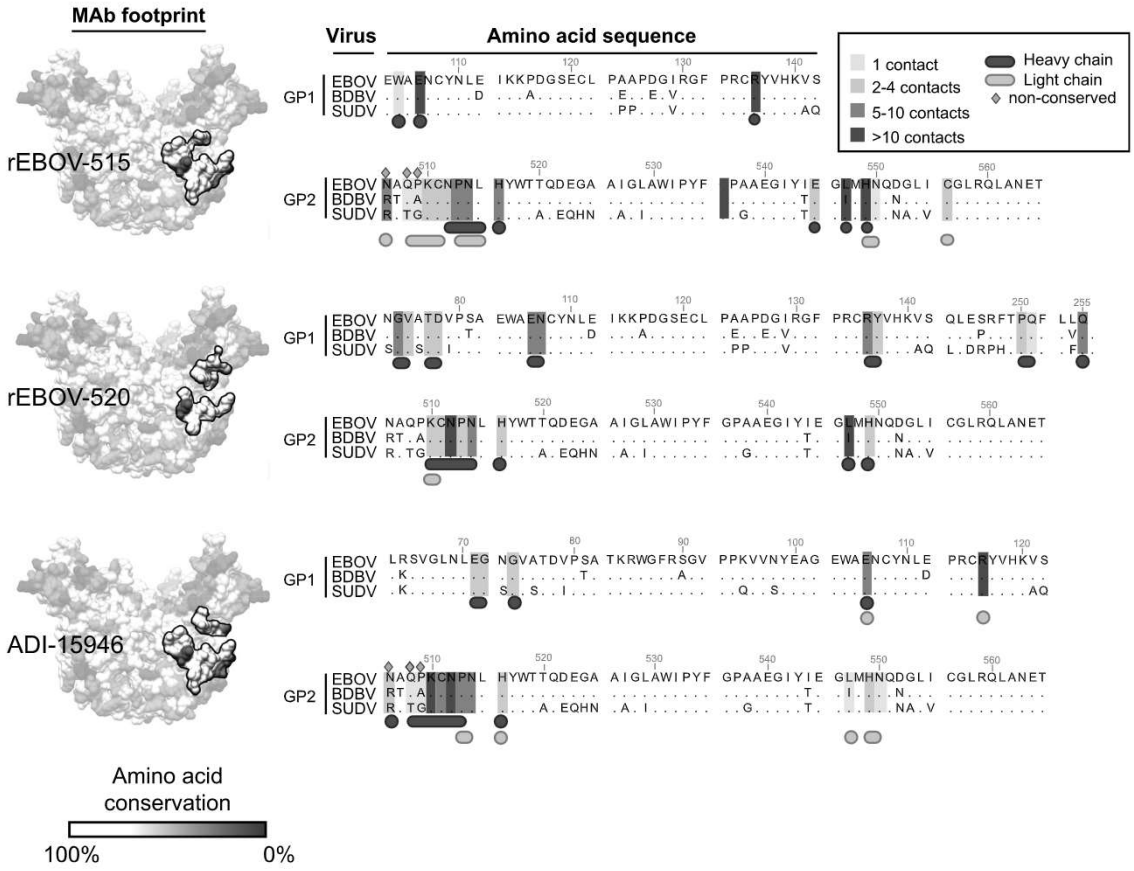

Figure 7. Conservation of the binding sites for broad mAbs rEBOV-515, rEBOV-520, and ADI-15946

Apo-GP is surface-rendered according to residue conservation on the left, with no conservation in dark purple (0%) and complete conservation in white (100%). The corresponding mAb footprints are highlighted. On the right are aligned sequences of the interacting regions on GP from EBOV, BDBV, and SUDV. Total contacts for each residue at 4 Å distance or less were determined (see Table S7), and residues are highlighted in blue according to the number of contacts, with darker blue indicating more contacts and thus a higher likelihood for contributing critically to binding. Residues that are variable are marked with a green diamond. HC contacts are indicated below in dark purple and LC contacts in pink.

cleavage loop compared to that caused by rEBOV-520, which may explain the high cell surface-displayed GP cleavage-inhibiting activity of EBOV-515 (Figure S7B). Further, a distinct pose of rEBOV-515 binding into the 3_{10} pocket avoids clashes with the α2 helix of the glycan cap (Figure 6F), unlike the binding of rEBOV-520 to the GP, which requires the α2 helix shift (Gilchuk et al., 2020b). This finding suggested that the binding site of rEBOV-515 on the intact GP molecule is more accessible than the rEBOV-520 binding site, which could explain the higher neutralizing potency of rEBOV-515 when compared to the potency of rEBOV-520 against the virus carrying the intact GP as we reported previously (Gilchuk et al., 2018a). Of note, we have shown previously that GP cleavage, which removes the glycan cap along with the β17-β18 loop, resulted in enhanced binding to cell-surface-displayed cleaved GP and increased neutralizing potency for both rEBOV-515 and rEBOV-520 (Gilchuk et al., 2018a, 2020b).

There are notable differences in degree of pan-ebolavirus neutralization and protection by each of three reported broadly reactive human mAbs despite recognition of partially overlapped epitopes they recognize on the GP base (Figure 6B). ADI-15946 did not fully neutralize most antigenically distinct SUDV (Wec et al., 2017; West et al., 2019), rEBOV-520 neutralized SUDV with modest potency but showed weak protection against SUDV in mice, and rEBOV-515 potently neutralized each of three viruses and protected against SUDV in mice (Gilchuk et al., 2018a, 2020b). Our structural analysis allowed us to compare the epitope footprint and contacts for each of these antibodies in relation to sequence conservation between the three major ebolavirus (Figures 7 and S6), providing insight that may help explain differences in neutralization breadth. ADI-15946 makes fewer contacts with GP1 but more contacts to the N terminus of GP2, a region that is less conserved that may explain weak SUDV neutralization. Conversely, rEBOV-520 makes more extensive contacts with GP1, because this region is generally less conserved. rEBOV-515 relies on minimal contacts with GP1, except in regions that are completely conserved, including R136 and E106. Taken together with a more conserved footprint, these observations provide a molecular basis for the superior breadth of neutralization and protection exhibited by rEBOV-515 over similar mAbs.

DISCUSSION

Here, we report comprehensive studies of pan-ebolavirus mAb cocktail treatment with a well-defined and complex molecular basis of broad neutralization and potency. The cocktail exhibited high therapeutic efficacy against all three medically important ebolaviruses in nonhuman primates. The discovery and recent approval of human mAb-based therapeutics represents a landmark achievement in the development of EVD medical countermeasures. The clinical trials in the DRC outbreak, however, highlighted that substantial gaps remained in improving the treatment of acute EVD (Iversen et al., 2020). The greatest benefit of mAb treatment in patients was mainly in those receiving early therapy, and only moderate benefit was observed in severely ill patients (Levine, 2019). Another remaining challenge for implementation of the current regimens is the logistical complexity of intravenous drug administration in the field, which may limit widespread application of mAb therapy in future outbreak scenarios.

Given the difference in efficacy mediated by different mAb drugs that was observed for advanced EVD treatments, mAb potency likely is a key contributing determinant of treatment efficacy. Inmazeb and Ebanga demonstrated higher efficacy when compared to that of the mAb cocktail ZMapp in clinical trials (Levine, 2019). Inmazeb is a three-antibody cocktail based on REGN-EB3 mAb sequences (Pascal et al., 2018), Ebanga is a monotherapy based on the antibody mAb114 (Corti et al., 2016), and ZMapp is a cocktail of three murine-human chimeric mAbs (Qiu et al., 2014). A comparison with the historical NHPs studies with REGN-EB3 (3 × 50 mg/kg dose at days 5, 8, and 11 after exposure) (Pascal et al., 2018), mAb114 (3 × 50 mg/kg dose at days 1, 2, and 3 after exposure) (Corti et al., 2016), and ZMapp (3 × 50 mg/kg dose at days 3, 6, and 9 after exposure) (Qiu et al., 2014) suggested equivalent or likely higher potency of our EBOV-442 IgG1 + EBOV-515 LALA-PG cocktail treatment (2 × 30 mg/kg at days 3 and 6 after exposure) against homologous EBOV. More studies are needed to compare available treatments and to determine if increasing mAb therapeutic potency would benefit clinical outcomes in treatment of severely ill patients and/or allow for rapid and more practical treatment by an alternative (intramuscular or subcutaneous) route of mAb delivery.

Broadly reactive mouse (Furuyama et al., 2016; Holtsberg et al., 2015), macaque (Keck et al., 2016; Zhao et al., 2017), and human (Flyak et al., 2016; Zhao et al., 2017) mAbs that exhibited varying degrees of EBOV, BDBV, and SUDV cross-neutralization and protection *in vivo* have been reported. One of the most well-characterized broadly neutralizing mAbs is the macaque mAb CA45 that also demonstrated broad protection in animals (Zhao et al., 2017). Anticipation of future EVD outbreaks requires consideration of therapeutic breadth, and mAbs of human origin are most suitable for the development of human therapeutics. As an added feature, the two-antibody cocktail we describe here offered an increased therapeutic breadth that extended to protection against BDBV and SUDV in NHP models. One other investigational human mAb cocktail that demonstrated broad efficacy in NHPs, $MBP134^{AF}$, has been described (Bornholdt et al., 2019). $MBP134^{AF}$ is comprised of mAb ADI-15878 and a derivative of mAb ADI-15946 (defined as ADI-23774), which was engineered to improve its specificity against SUDV GP (Wec et al., 2019). A comparison of our results to the reported activities of ADI-15946 or ADI-23774 (Wec et al., 2017) indicates a high potency for the homologous base-specific mAb rEBOV-515 that we describe. In agreement with this functional assessment, our structural data showed that rEBOV-515 strongly interacts with conserved residues in the GP, with a unique footprint among base-specific broadly reactive human mAbs rEBOV-515, rEBOV-520, and ADI-15946, suggesting a structural basis for its remarkable breadth and potency. In addition, the analysis revealed features that are essential for synergistic and efficient GP binding in the cocktail of rEBOV-515 + rEBOV-442 but distinct from those in the cocktail of rEBOV-520 + rEBOV-548 we previously described. First, there is a reciprocal enhancement of the GP binding in the cocktail of rEBOV-515 + rEBOV-442. Second, binding to the GP occurs without major structural remodeling of the GP1 while displacing the β17-β18 loop from the binding site of rEBOV-515. Together, this suggests a mechanism for high neutralization potency in the cocktail.

Multifunctionality is another desirable feature in mAb cocktails in addition to neutralizing potency and breadth (Saphire et al., 2018). Reports of human EVD cases revealed high plasma viral RNA titers at the time of patient admission into mAb treatment studies (Brown et al., 2018; Mbala-Kingebeni et al., 2019). Similarly, we observed high serum viral titers in each cohort of challenged NHPs before mAb treatment (Figure 5), indicating that at the time of treatment many cells in multiple organs are already infected. This finding highlights the importance to retain Fc-mediated effector function activity in mAb cocktails in order to preserve the ability to eliminate infected cells. Conversely, using mouse challenge models we demonstrated that the complementary Fc-region-mediated functions of rEBOV-515-like neutralizing mAbs measured by *in vitro* assays do not benefit therapeutic efficacy but instead resulted in lower levels of *in vivo* protection. In the cocktails of EBOV-442 IgG1 + EBOV-515 LALA-PG, the stronger and broader neutralizing mAb EBOV-515 LALA-PG may act directly to neutralize circulating virus, and this activity is enhanced synergistically in the presence of rEBOV-442 IgG1. rEBOV-442 IgG1, in addition to direct virus neutralization, may act through Fc-mediated functions by binding to the non-overlapping antigenic site on the GP on infected cells, and this activity could be enhanced reciprocally in the presence of EBOV-515 LALA-PG. Such a combination of activities may facilitate viral clearance and potentially decrease the likelihood of viral mutations that facilitate escape from the cocktail treatment. The relative contribution of these activities to the therapeutic efficacy exhibited by this cocktail needs further investigation.

Defining the likelihood of the viral escape for clinical candidate mAbs has important implications for predicting therapeutic efficacy following mAb treatment (Copin et al., 2021). Our study suggests that individual mAbs may differ in their ability to limit the occurrence of escape variants and showed ''orthogonality'' of the escape mutations for broadly neutralizing mAbs we tested. In an outbreak scenario, implementation of several broad cocktails exhibiting such complementary neutralizing activities may safeguard against escape mutant selection in the population.

During acute EVD, circulating infectious virus sometimes seeds immune-privileged tissues, including the brain, eyes, and testes, and persist after clearance from the blood and recovery (Diallo et al., 2016; Subtil et al., 2017; Varkey et al., 2015). Until recently, it was generally assumed that Ebola epidemics start upon zoonotic transmission. On February 14, 2021, a new EVD outbreak was declared in Guinea, and viral genome sequencing reports suggested that the outbreak was caused by the Makona variant of EBOV that caused the 2014 EVD epidemics (Keita et al., 2021). The index case of the 2021 Guinea cluster likely was infected from a persistent source, such as via sexual transmission from an EVD survivor (Keita et al., 2021) raising concerns about possible person-to-person transmission and reignition of outbreaks. The existing therapies and those that are currently in clinical development should be evaluated for their efficacy in clearing infectious virus from immune-privileged sites. Further, NHP studies suggested a genetic drift upon selection pressure with sub-optimal mAb treatment that could be a potential cause for failure during EVD treatment (Kugelman et al., 2015). Potent mAb cocktails like EBOV-442 IgG1 + EBOV-515 LALA-PG may help thwart antigenic drift by targeting non-overlapping vulnerable sites on GP and exhibiting complementary mechanisms of action.

In summary, these studies highlight the power of implementing a rational mAb cocktail development program using structure-function-guided principles (e.g., knowledge of binding sites, neutralization breadth, resistance to escape, multifunctionality, synergy, etc.). We identified a pan-ebolavirus biologic comprising a two-antibody cocktail that exhibits high efficacy for treatment of all three medically important ebolaviruses. These findings set the stage for clinical evaluation of pan-ebolavirus combination therapy with the two human antibodies rEBOV-442 IgG1 and rEBOV-515 LALA-PG.

Limitations of study

The degree to which the Fc-region mediated effector functions studied in animal models using fully human EBOV-442 IgG1 and rEBOV-515 LALA-PG mAbs translated into a therapeutic potential by these mAbs against human EVD is unknown and should be further investigated. The protection of NHPs from advanced EVD by the described mAb cocktail treatment should be assessed in future studies. The developability (manufacturability) of antibodies described here needs to be assessed in future studies.

STAR★METHODS

Detailed methods are provided in the online version of this paper and include the following:

- KEY RESOURCES TABLE
- RESOURCE AVAILABILITY
  - Lead contact
  - Materials availability
  - Data and code availability
- EXPERIMENTAL MODEL AND SUBJECT DETAILS
  - Cell lines
  - Viruses
  - Mouse model
  - Nonhuman primate (NHP) model
- METHOD DETAILS
  - Monoclonal antibody production and purification
  - GP expression and purification
  - ELISA binding assay
  - Mammalian cell-surface-displayed GP antibody binding
  - Measurement of synergistic GP binding by a combination of antibodies
  - Selection and sequencing of VSV/EBOV GP mutants that escape antibody neutralization
  - Neutralization assays
  - Measurement of synergistic virus neutralization by a combination of antibodies
  - Rapid fluorometric antibody-mediated cytotoxicity assay (RFADCC)
  - GP cleavage inhibition
  - Mouse challenge
  - NHP challenge
  - Measurement of virus load in NHP blood and tissues
  - NHP serum biochemistry
  - Sample preparation for cryogenic electron microscopy
  - Cryogenic electron microscopy data collection and processing
  - Cryogenic electron microscopy model building and refinement
- QUANTIFICATION AND STATISTICAL ANALYSIS

SUPPLEMENTAL INFORMATION

Supplemental information can be found online at https://doi.org/10.1016/j.cell.2021.09.035.

ACKNOWLEDGMENTS

We thank D. Deer for technical assistance with NHP studies. We thank George K. Lewis, Robin Flinko, and Chiara Orlandi for providing target cell line and protocols for RFADCC assay. The Jurkat-EBOV GP cell line was a kind gift from C. Davis and R. Ahmed. This work was supported by NIH (U19 AI109711 to J.E.C. and A.B., U19 AI142785 to J.E.C. and T.W.G., and U19 AI109762 to A.B.W.), HHS (HHSN272201400058C to J.E.C.), and DTRA (HDTRA1-13-1-0034 to J.E.C. and A.B.). J.E.C. is a recipient of the 2019 Future Insight Prize from Merck KGaA, which supported this work with a grant. The project was supported by The Vanderbilt Institute for Clinical and Translational Research (VICTR) funded by the National Center for Advancing Translational Sciences (NCATS) Clinical Translational Science Award (CTSA) Program (5UL1TR002243-03). Work in BSL-4 and ABSL-4 was supported by NIH (5UC7AI094660-07) and by the Animal Resource Center of the Galveston National Laboratory. The content is solely the responsibility of the authors and does not necessarily represent the official views of the NIH.

AUTHOR CONTRIBUTIONS

P.G., C.D.M., R.W.C., R.H.C., A.B., T.W.G., A.B.W., and J.E.C. planned the studies. P.G., C.D.M., R.W.C., P.A.I., K.H., V.B., K.N.A., J.B.G., N.K., T.A., R.S.N., R.E.S., N.S., S.J.Z., and R.G.B. conducted experiments. P.G., C.D.M., R.W.C., A.B., T.W.G., A.B.W., and J.E.C. interpreted the studies. P.G., C.D.M., and J.E.C. wrote the first draft of the paper. A.B., T.W.G., A.B.W, and J.E.C. obtained funding. All authors reviewed, edited, and approved the paper.

DECLARATION OF INTERESTS

J.E.C. has served as a consultant for Eli Lilly, GlaxoSmithKline and Luna Biologics, is a member of the Scientific Advisory Boards of CompuVax and Meissa Vaccines, and is Founder of IDBiologics. The Crowe laboratory at Vanderbilt University Medical Center has received unrelated sponsored research agreements from Takeda Vaccines, IDBiologics, and AstraZeneca. Vanderbilt University has applied for patents concerning ebolavirus antibodies that are related to this work. All other authors declare no competing interests.

Received: April 6, 2021
Revised: July 27, 2021
Accepted: September 27, 2021
Published: October 28, 2021

REFERENCES

Agirre, J., Iglesias-Fernández, J., Rovira, C., Davies, G.J., Wilson, K.S., and Cowtan, K.D. (2015). Privateer: software for the conformational validation of carbohydrate structures. Nat. Struct. Mol. Biol. *22*, 833–834.

Barad, B.A., Echols, N., Wang, R.Y., Cheng, Y., DiMaio, F., Adams, P.D., and Fraser, J.S. (2015). EMRinger: side chain-directed model and map validation for 3D cryo-electron microscopy. Nat. Methods *12*, 943–946.

Baum, A., Fulton, B.O., Wloga, E., Copin, R., Pascal, K.E., Russo, V., Giordano, S., Lanza, K., Negron, N., Ni, M., et al. (2020). Antibody cocktail to SARS-CoV-2 spike protein prevents rapid mutational escape seen with individual antibodies. Science *369*, 1014–1018.

Bennett, R.S., Huzella, L.M., Jahrling, P.B., Bollinger, L., Olinger, G.G., Jr., and Hensley, L.E. (2017). Nonhuman primate models of Ebola virus disease. Curr. Top. Microbiol. Immunol. *411*, 171–193.

Biasini, M., Bienert, S., Waterhouse, A., Arnold, K., Studer, G., Schmidt, T., Kiefer, F., Gallo Cassarino, T., Bertoni, M., Bordoli, L., and Schwede, T. (2014). SWISS-MODEL: modelling protein tertiary and quaternary structure using evolutionary information. Nucleic Acids Res. *42*, W252-8.

Bornholdt, Z.A., Ndungo, E., Fusco, M.L., Bale, S., Flyak, A.I., Crowe, J.E., Jr., Chandran, K., and Saphire, E.O. (2016). Host-primed Ebola virus GP exposes a hydrophobic NPC1 receptor-binding pocket, revealing a target for broadly neutralizing antibodies. MBio *7*, e02154-15.

Bornholdt, Z.A., Herbert, A.S., Mire, C.E., He, S., Cross, R.W., Wec, A.Z., Abelson, D.M., Geisbert, J.B., James, R.M., Rahim, M.N., et al. (2019). A two-antibody pan-ebolavirus cocktail confers broad therapeutic protection in ferrets and nonhuman primates. Cell Host Microbe *25*, 49–58.e5.

Bray, M., Davis, K., Geisbert, T., Schmaljohn, C., and Huggins, J. (1998). A mouse model for evaluation of prophylaxis and therapy of Ebola hemorrhagic fever. J. Infect. Dis. *178*, 651–661.

Brown, J.F., Dye, J.M., Tozay, S., Jeh-Mulbah, G., Wohl, D.A., Fischer, W.A., 2nd, Cunningham, C.K., Rowe, K., Zacharias, P., van Hasselt, J., et al. (2018). Anti-Ebola virus antibody levels in convalescent plasma and viral load after plasma infusion in patients with Ebola virus disease. J. Infect. Dis. *218*, 555–562.

Carette, J.E., Raaben, M., Wong, A.C., Herbert, A.S., Obernosterer, G., Mulherkar, N., Kuehne, A.I., Kranzusch, P.J., Griffin, A.M., Ruthel, G., et al. (2011). Ebola virus entry requires the cholesterol transporter Niemann-Pick C1. Nature *477*, 340–343.

Chandran, K., Sullivan, N.J., Felbor, U., Whelan, S.P., and Cunningham, J.M. (2005). Endosomal proteolysis of the Ebola virus glycoprotein is necessary for infection. Science *308*, 1643–1645.

Chng, J., Wang, T., Nian, R., Lau, A., Hoi, K.M., Ho, S.C., Gagnon, P., Bi, X., and Yang, Y. (2015). Cleavage efficient 2A peptides for high level monoclonal antibody expression in CHO cells. MAbs *7*, 403–412.

Copin, R., Baum, A., Wloga, E., Pascal, K.E., Giordano, S., Fulton, B.O., Zhou, A., Negron, N., Lanza, K., Chan, N., et al. (2021). The monoclonal antibody combination REGEN-COV protects against SARS-CoV-2 mutational escape in preclinical and human studies. Cell *184*, 3949–3961.

Corti, D., Misasi, J., Mulangu, S., Stanley, D.A., Kanekiyo, M., Wollen, S., Ploquin, A., Doria-Rose, N.A., Staupe, R.P., Bailey, M., et al. (2016). Protective monotherapy against lethal Ebola virus infection by a potently neutralizing antibody. Science *351*, 1339–1342.

Cross, R.W., Mire, C.E., Borisevich, V., Geisbert, J.B., Fenton, K.A., and Geisbert, T.W. (2016). The Domestic Ferret (Mustela putorius furo) as a lethal infection model for 3 species of ebolavirus. J. Infect. Dis. *214*, 565–569.

Davis, C.W., Jackson, K.J.L., McElroy, A.K., Halfmann, P., Huang, J., Chennareddy, C., Piper, A.E., Leung, Y., Albarino, C.G., Crozier, I., et al. (2019). Longitudinal analysis of the human B cell response to Ebola virus infection. Cell *177*, 1566–1582.

Diallo, B., Sissoko, D., Loman, N.J., Bah, H.A., Bah, H., Worrell, M.C., Conde, L.S., Sacko, R., Mesfin, S., Loua, A., et al. (2016). Resurgence of Ebola virus disease in Guinea linked to a survivor with virus persistence in seminal fluid for more than 500 days. Clin. Infect. Dis. *63*, 1353–1356.

DiMaio, F., Song, Y., Li, X., Brunner, M.J., Xu, C., Conticello, V., Egelman, E., Marlovits, T., Cheng, Y., and Baker, D. (2015). Atomic-accuracy models from 4.5-Å cryo-electron microscopy data with density-guided iterative local refinement. Nat. Methods *12*, 361–365.

Domi, A., Feldmann, F., Basu, R., McCurley, N., Shifflett, K., Emanuel, J., Hellerstein, M.S., Guirakhoo, F., Orlandi, C., Flinko, R., et al. (2018). A single dose of modified Vaccinia Ankara expressing Ebola virus like particles protects nonhuman primates from lethal Ebola virus challenge. Sci. Rep. *8*, 864.

Emsley, P., Lohkamp, B., Scott, W.G., and Cowtan, K. (2010). Features and development of Coot. Acta Crystallogr. D Biol. Crystallogr. *66*, 486–501.

Feldmann, H., Sprecher, A., and Geisbert, T.W. (2020). Ebola. N. Engl. J. Med. *382*, 1832–1842.

Fibriansah, G., Ibarra, K.D., Ng, T.S., Smith, S.A., Tan, J.L., Lim, X.N., Ooi, J.S.G., Kostyuchenko, V.A., Wang, J., de Silva, A.M., et al. (2015). DENGUE VIRUS. Cryo-EM structure of an antibody that neutralizes dengue virus type 2 by locking E protein dimers. Science *349*, 88–91.

Flyak, A.I., Shen, X., Murin, C.D., Turner, H.L., David, J.A., Fusco, M.L., Lampley, R., Kose, N., Ilinykh, P.A., Kuzmina, N., et al. (2016). Cross-reactive and potent neutralizing antibody responses in human survivors of natural ebolavirus infection. Cell *164*, 392–405.

Food and Drug Administration (2020a). FDA Approves First Treatment for Ebola Virus. https://www.fdagov/news-events/press-announcements/fda-approves-first-treatment-ebola-virus.

Food and Drug Administration (2020b). FDA Approves Treatment for Ebola Virus. https://www.fdagov/drugs/drug-safety-and-availability/fda-approves-treatment-ebola-virus.

Furuyama, W., Marzi, A., Nanbo, A., Haddock, E., Maruyama, J., Miyamoto, H., Igarashi, M., Yoshida, R., Noyori, O., Feldmann, H., and Takada, A. (2016). Discovery of an antibody for pan-ebolavirus therapy. Sci. Rep. *6*, 20514.

Garbutt, M., Liebscher, R., Wahl-Jensen, V., Jones, S., Möller, P., Wagner, R., Volchkov, V., Klenk, H.D., Feldmann, H., and Ströher, U. (2004). Properties of replication-competent vesicular stomatitis virus vectors expressing glycoproteins of filoviruses and arenaviruses. J. Virol. *78*, 5458–5465.

Gaudinski, M.R., Coates, E.E., Novik, L., Widge, A., Houser, K.V., Burch, E., Holman, L.A., Gordon, I.J., Chen, G.L., Carter, C., et al.; VRC 608 Study team (2019). Safety, tolerability, pharmacokinetics, and immunogenicity of the therapeutic monoclonal antibody mAb114 targeting Ebola virus glycoprotein (VRC 608): an open-label phase 1 study. Lancet *393*, 889–898.

Geisbert, T.W., Daddario-DiCaprio, K.M., Williams, K.J., Geisbert, J.B., Leung, A., Feldmann, F., Hensley, L.E., Feldmann, H., and Jones, S.M. (2008). Recombinant vesicular stomatitis virus vector mediates postexposure protection against Sudan Ebola hemorrhagic fever in nonhuman primates. J. Virol. *82*, 5664–5668.

Geisbert, T.W., Strong, J.E., and Feldmann, H. (2015). Considerations in the use of nonhuman primate models of Ebola virus and Marburg virus infection. J. Infect. Dis. *212* (*Suppl 2*), S91–S97.

Gilchuk, P., Kuzmina, N., Ilinykh, P.A., Huang, K., Gunn, B.M., Bryan, A., Davidson, E., Doranz, B.J., Turner, H.L., Fusco, M.L., et al. (2018a). Multifunctional pan-ebolavirus antibody recognizes a site of broad vulnerability on the Ebolavirus glycoprotein. Immunity *49*, 363–374.e10.

Gilchuk, P., Mire, C.E., Geisbert, J.B., Agans, K.N., Deer, D.J., Cross, R.W., Slaughter, J.C., Flyak, A.I., Mani, J., Pauly, M.H., et al. (2018b). Efficacy of human monoclonal antibody monotherapy against Bundibugyo virus infection in nonhuman primates. J. Infect. Dis. *218* (*Suppl 5*), S565–S573.

Gilchuk, P., Bombardi, R.G., Erasmus, J.H., Tan, Q., Nargi, R., Soto, C., Abbink, P., Suscovich, T.J., Durnell, L.A., Khandhar, A., et al. (2020a). Integrated pipeline for the accelerated discovery of antiviral antibody therapeutics. Nat. Biomed. Eng. *4*, 1030–1043.

Gilchuk, P., Murin, C.D., Milligan, J.C., Cross, R.W., Mire, C.E., Ilinykh, P.A., Huang, K., Kuzmina, N., Altman, P.X., Hui, S., et al. (2020b). Analysis of a therapeutic antibody cocktail reveals determinants for cooperative and broad ebolavirus neutralization. Immunity *52*, 388–403.e12.

Goldstein, T., Anthony, S.J., Gbakima, A., Bird, B.H., Bangura, J., Tremeau-Bravard, A., Belaganahalli, M.N., Wells, H.L., Dhanota, J.K., Liang, E., et al. (2018). The discovery of Bombali virus adds further support for bats as hosts of ebolaviruses. Nat. Microbiol. *3*, 1084–1089.

Greaney, A.J., Starr, T.N., Gilchuk, P., Zost, S.J., Binshtein, E., Loes, A.N., Hilton, S.K., Huddleston, J., Eguia, R., Crawford, K.H.D., et al. (2021). Complete mapping of mutations to the SARS-CoV-2 spike receptor-binding domain that escape antibody recognition. Cell Host Microbe *29*, 44–57.e9.

Herbert, A.S., Froude, J.W., Ortiz, R.A., Kuehne, A.I., Dorosky, D.E., Bakken, R.R., Zak, S.E., Josleyn, N.M., Musiychuk, K., Jones, R.M., et al. (2020). Development of an antibody cocktail for treatment of Sudan virus infection. Proc. Natl. Acad. Sci. USA *117*, 3768–3778.

Holtsberg, F.W., Shulenin, S., Vu, H., Howell, K.A., Patel, S.J., Gunn, B., Karim, M., Lai, J.R., Frei, J.C., Nyakatura, E.K., et al. (2015). Pan-ebolavirus and pan-filovirus mouse monoclonal antibodies: protection against Ebola and Sudan viruses. J. Virol. *90*, 266–278.

Ianevski, A., Giri, A.K., and Aittokallio, T. (2020). SynergyFinder 2.0: visual analytics of multi-drug combination synergies. Nucleic Acids Res. *48* (W1), W488–W493.

Ilinykh, P.A., Shen, X., Flyak, A.I., Kuzmina, N., Ksiazek, T.G., Crowe, J.E., Jr., and Bukreyev, A. (2016). Chimeric filoviruses for identification and characterization of monoclonal antibodies. J. Virol. *90*, 3890–3901.

Iversen, P.L., Kane, C.D., Zeng, X., Panchal, R.G., Warren, T.K., Radoshitzky, S.R., Kuhn, J.H., Mudhasani, R.R., Cooper, C.L., Shurtleff, A.C., et al. (2020). Recent successes in therapeutics for Ebola virus disease: no time for complacency. Lancet Infect. Dis. *20*, e231–e237.

Jubb, H.C., Higueruelo, A.P., Ochoa-Montaño, B., Pitt, W.R., Ascher, D.B., and Blundell, T.L. (2017). Arpeggio: A web server for calculating and visualising interatomic interactions in protein structures. J. Mol. Biol. *429*, 365–371.

King, L.B., West, B.R., Schendel, S.L., and Saphire, E.O. (2018). The structural basis for filovirus neutralization by monoclonal antibodies. Curr. Opin. Immunol. *53*, 196–202.

Keck, Z.Y., Enterlein, S.G., Howell, Howell, Vu, H., Shulenin, S., Froude, J.W., Araghi, N., Douglas, R., Biggins, J., et al. (2016). Macaque monoclonal antibodies targeting novel conserved epitopes within filovirus glycoprotein. J. Virol *90*, 279–291.

Keita, A.K., Koundouno, F.R., Faye, M., Dux, A., Hinzmann, J., Diallo, H., Ayouba, A., Le Marcis, F., Soropogui, B., Ifono, K., et al. (2021). Resurgence of Ebola virus in 2021 in Guinea suggests a new paradigm for outbreaks. Nature *597*, 539–543.

King, L.B., Milligan, J.C., West, B.R., Schendel, S.L., and Ollmann Saphire, E. (2019). Achieving cross-reactivity with pan-ebolavirus antibodies. Curr. Opin. Virol. *34*, 140–148.

Kugelman, J.R., Kugelman-Tonos, J., Ladner, J.T., Pettit, J., Keeton, C.M., Nagle, E.R., Garcia, K.Y., Froude, J.W., Kuehne, A.I., Kuhn, J.H., et al. (2015). Emergence of Ebola virus escape variants in infected nonhuman primates treated with the MB-003 antibody cocktail. Cell Rep. *12*, 2111–2120.

Kuhn, J.H., Adachi, T., Adhikari, N.K.J., Arribas, J.R., Bah, I.E., Bausch, D.G., Bhadelia, N., Borchert, M., Brantsæter, A.B., Brett-Major, D.M., et al. (2019). New filovirus disease classification and nomenclature. Nat. Rev. Microbiol. *17*, 261–263.

Kuzmina, N.A., Younan, P., Gilchuk, P., Santos, R.I., Flyak, A.I., Ilinykh, P.A., Huang, K., Lubaki, N.M., Ramanathan, P., Crowe, J.E., Jr., et al. (2018). Antibody-dependent enhancement of Ebola virus infection by human antibodies isolated from survivors. Cell Rep. *24*, 1802–1815.

Laskowski, R.A., and Swindells, M.B. (2011). LigPlot+: multiple ligand-protein interaction diagrams for drug discovery. J. Chem. Inf. Model. *51*, 2778–2786.

Lee, J.E., and Saphire, E.O. (2009). Neutralizing ebolavirus: structural insights into the envelope glycoprotein and antibodies targeted against it. Curr. Opin. Struct. Biol. *19*, 408–417.

Lee, J.E., Fusco, M.L., Hessell, A.J., Oswald, W.B., Burton, D.R., and Saphire, E.O. (2008). Structure of the Ebola virus glycoprotein bound to an antibody from a human survivor. Nature *454*, 177–182.

Levine, M.M. (2019). Monoclonal antibody therapy for Ebola virus disease. N. Engl. J. Med. *381*, 2365–2366.

Liebschner, D., Afonine, P.V., Baker, M.L., Bunkóczi, G., Chen, V.B., Croll, T.I., Hintze, B., Hung, L.W., Jain, S., McCoy, A.J., et al. (2019). Macromolecular structure determination using X-rays, neutrons and electrons: recent developments in Phenix. Acta Crystallogr. D Struct. Biol. *75*, 861–877.

Lo, M., Kim, H.S., Tong, R.K., Bainbridge, T.W., Vernes, J.M., Zhang, Y., Lin, Y.L., Chung, S., Dennis, M.S., Zuchero, Y.J.Y., et al. (2017). Effector-attenuating substitutions that maintain antibody stability and reduce toxicity in mice. J. Biol. Chem. *292*, 3900–3908.

Lütteke, T., and von der Lieth, C.W. (2004). pdb-care (PDB carbohydrate residue check): a program to support annotation of complex carbohydrate structures in PDB files. BMC Bioinformatics *5*, 69.

Mbala-Kingebeni, P., Aziza, A., Di Paola, N., Wiley, M.R., Makiala-Mandanda, S., Caviness, K., Pratt, C.B., Ladner, J.T., Kugelman, J.R., Prieto, K., et al. (2019). Medical countermeasures during the 2018 Ebola virus disease outbreak in the North Kivu and Ituri Provinces of the Democratic Republic of the Congo: a rapid genomic assessment. Lancet Infect. Dis. *19*, 648–657.

Mire, C.E., Geisbert, J.B., Marzi, A., Agans, K.N., Feldmann, H., and Geisbert, T.W. (2013). Vesicular stomatitis virus-based vaccines protect nonhuman primates against Bundibugyo ebolavirus. PLoS Negl. Trop. Dis. *7*, e2600.

Misasi, J., and Sullivan, N.J. (2021). Immunotherapeutic strategies to target vulnerabilities in the Ebolavirus glycoprotein. Immunity *54*, 412–436.

Mulangu, S., Dodd, L.E., Davey, R.T., Jr., Tshiani Mbaya, O., Proschan, M., Mukadi, D., Lusakibanza Manzo, M., Nzolo, D., Tshomba Oloma, A., Ibanda, A., et al.; PALM Writing Group; PALM Consortium Study Team (2019). A randomized, controlled trial of Ebola virus disease therapeutics. N. Engl. J. Med. *381*, 2293–2303.

Murin, C.D., Gilchuk, P., Ilinykh, P.A., Huang, K., Kuzmina, N., Shen, X., Bruhn, J.F., Bryan, A.L., Davidson, E., Doranz, B.J., et al. (2021). Convergence of a common solution for broad ebolavirus neutralization by glycan cap-directed human antibodies. Cell Rep. *35*, 108984.

Orlandi, C., Flinko, R., and Lewis, G.K. (2016). A new cell line for high throughput HIV-specific antibody-dependent cellular cytotoxicity (ADCC) and cell-to-cell virus transmission studies. J. Immunol. Methods *433*, 51–58.

Oswald, W.B., Geisbert, T.W., Davis, K.J., Geisbert, J.B., Sullivan, N.J., Jahrling, P.B., Parren, P.W., and Burton, D.R. (2007). Neutralizing antibody fails to impact the course of Ebola virus infection in monkeys. PLoS Pathog. *3*, e9.

Pascal, K.E., Dudgeon, D., Trefry, J.C., Anantpadma, M., Sakurai, Y., Murin, C.D., Turner, H.L., Fairhurst, J., Torres, M., Rafique, A., et al. (2018). Development of clinical-stage human monoclonal antibodies that treat advanced Ebola virus disease in nonhuman primates. J. Infect. Dis. *218* (*Suppl 5*), S612–S626.

Pettersen, E.F., Goddard, T.D., Huang, C.C., Couch, G.S., Greenblatt, D.M., Meng, E.C., and Ferrin, T.E. (2004). UCSF Chimera–a visualization system for exploratory research and analysis. J. Comput. Chem. *25*, 1605–1612.

Punjani, A., Rubinstein, J.L., Fleet, D.J., and Brubaker, M.A. (2017). cryoSPARC: algorithms for rapid unsupervised cryo-EM structure determination. Nat. Methods *14*, 290–296.

Qiu, X., Wong, G., Audet, J., Bello, A., Fernando, L., Alimonti, J.B., Fausther-Bovendo, H., Wei, H., Aviles, J., Hiatt, E., et al. (2014). Reversion of advanced Ebola virus disease in nonhuman primates with ZMapp. Nature *514*, 47–53.

Sanchez, A., and Rollin, P.E. (2005). Complete genome sequence of an Ebola virus (Sudan species) responsible for a 2000 outbreak of human disease in Uganda. Virus Res. *113*, 16–25.

Saphire, E.O., Schendel, S.L., Fusco, M.L., Gangavarapu, K., Gunn, B.M., Wec, A.Z., Halfmann, P.J., Brannan, J.M., Herbert, A.S., Qiu, X., et al.; Viral Hemorrhagic Fever Immunotherapeutic Consortium (2018). Systematic analysis of monoclonal antibodies against Ebola virus GP defines features that contribute to protection. Cell *174*, 938–952.e13.

Sivapalasingam, S., Kamal, M., Slim, R., Hosain, R., Shao, W., Stoltz, R., Yen, J., Pologe, L.G., Cao, Y., Partridge, M., et al. (2018). Safety, pharmacokinetics, and immunogenicity of a co-formulated cocktail of three human monoclonal antibodies targeting Ebola virus glycoprotein in healthy adults: a randomised, first-in-human phase 1 study. Lancet Infect. Dis. *18*, 884–893.

Starr, T.N., Greaney, A.J., Dingens, A.S., and Bloom, J.D. (2021). Complete map of SARS-CoV-2 RBD mutations that escape the monoclonal antibody LY-CoV555 and its cocktail with LY-CoV016. Cell Rep. Med. *2*, 100255.

Subtil, F., Delaunay, C., Keita, A.K., Sow, M.S., Touré, A., Leroy, S., Msellati, P., Magassouba, N., Baize, S., Raoul, H., et al.; Postebogui Study Group (2017). Dynamics of Ebola RNA persistence in semen: a report from the postebogui cohort in Guinea. Clin. Infect. Dis. *64*, 1788–1790.

Thi, E.P., Lee, A.C., Geisbert, J.B., Ursic-Bedoya, R., Agans, K.N., Robbins, M., Deer, D.J., Fenton, K.A., Kondratowicz, A.S., MacLachlan, I., et al. (2016). Rescue of non-human primates from advanced Sudan ebolavirus infection with lipid encapsulated siRNA. Nat. Microbiol. *1*, 16142.

Towner, J.S., Paragas, J., Dover, J.E., Gupta, M., Goldsmith, C.S., Huggins, J.W., and Nichol, S.T. (2005). Generation of eGFP expressing recombinant Zaire ebolavirus for analysis of early pathogenesis events and high-throughput antiviral drug screening. Virology *332*, 20–27.

Towner, J.S., Sealy, T.K., Khristova, M.L., Albariño, C.G., Conlan, S., Reeder, S.A., Quan, P.L., Lipkin, W.I., Downing, R., Tappero, J.W., et al. (2008). Newly discovered ebola virus associated with hemorrhagic fever outbreak in Uganda. PLoS Pathog. *4*, e1000212.

Varkey, J.B., Shantha, J.G., Crozier, I., Kraft, C.S., Lyon, G.M., Mehta, A.K., Kumar, G., Smith, J.R., Kainulainen, M.H., Whitmer, S., et al. (2015). Persistence of Ebola virus in ocular fluid during convalescence. N. Engl. J. Med. *372*, 2423–2427.

Wang, P., Nair, M.S., Liu, L., Iketani, S., Luo, Y., Guo, Y., Wang, M., Yu, J., Zhang, B., Kwong, P.D., et al. (2021). Antibody resistance of SARS-CoV-2 variants B.1.351 and B.1.1.7. Nature *593*, 130–135. https://doi.org/10.1038/s41586-021-03398-2.

Wec, A.Z., Herbert, A.S., Murin, C.D., Nyakatura, E.K., Abelson, D.M., Fels, J.M., He, S., James, R.M., de La Vega, M.A., Zhu, W., et al. (2017). Antibodies from a human survivor define sites of vulnerability for broad protection against ebolaviruses. Cell *169*, 878–890.e15.

Wec, A.Z., Bornholdt, Z.A., He, S., Herbert, A.S., Goodwin, E., Wirchnianski, A.S., Gunn, B.M., Zhang, Z., Zhu, W., Liu, G., et al. (2019). Development of a human antibody cocktail that deploys multiple functions to confer pan-ebolavirus protection. Cell Host Microbe *25*, 39–48.e5.

West, B.R., Wec, A.Z., Moyer, C.L., Fusco, M.L., Ilinykh, P.A., Huang, K., Wirchnianski, A.S., James, R.M., Herbert, A.S., Hui, S., et al. (2019). Structural basis of broad ebolavirus neutralization by a human survivor antibody. Nat. Struct. Mol. Biol. *26*, 204–212.

World Health Organization (2021). Ebola virus disease. https://www.whoint/en/news-room/fact-sheets/detail/ebola-virus-disease.

Yewdell, J.W., Webster, R.G., and Gerhard, W.U. (1979). Antigenic variation in three distinct determinants of an influenza type A haemagglutinin molecule. Nature *279*, 246–248.

Zhang, K. (2016). Gctf: Real-time CTF determination and correction. J. Struct. Biol. *193*, 1–12.

Zhao, X., Howell, K.A., He, S., Brannan, J.M., Wec, A.Z., Davidson, E., Turner, H.L., Chiang, C.I., Lei, L., Fels, J.M., et al. (2017). Immunization-elicited broadly protective antibody reveals ebolavirus fusion loop as a site of vulnerability. Cell *169*, 891–904.e15.

Zheng, S.Q., Palovcak, E., Armache, J.P., Verba, K.A., Cheng, Y., and Agard, D.A. (2017). MotionCor2: anisotropic correction of beam-induced motion for improved cryo-electron microscopy. Nat. Methods *14*, 331–332.

Zivanov, J., Nakane, T., Forsberg, B.O., Kimanius, D., Hagen, W.J., Lindahl, E., and Scheres, S.H. (2018). New tools for automated high-resolution cryo-EM structure determination in RELION-3. eLife *7*, e42166.

STAR★METHODS

KEY RESOURCES TABLE

REAGENT or RESOURCE	SOURCE	IDENTIFIER
Antibodies		
rEBOV-515 IgG1 (recombinant CHO-produced)	This study	N/A
rEBOV-515 LALA-PG (recombinant CHO-produced)	This study	N/A
rEBOV-442 IgG1 (recombinant CHO-produced)	This paper	N/A
rEBOV-442 LALA-PG (recombinant CHO-produced)	This paper	N/A
ADI-15878 IgG1 (recombinant CHO-produced); heavy chain V region	Wec et al., 2017	GenBank: KU602365
ADI-15878 IgG1 (recombinant CHO-produced); light chain V region	Wec et al., 2017	GenBank: KU602366
ADI-15946 IgG1 (recombinant CHO-produced); heavy chain V region	Wec et al., 2017	GenBank: KU602499
ADI-15946 IgG1 (recombinant CHO-produced); light chain V region	Wec et al., 2017	GenBank: KU602500
rDENV 2D22 (recombinant CHO-produced)	Fibriansah et al., 2015	N/A
Goat anti-human IgG-HRP	Southern Biotech	Cat# 2040-05; RRID:AB_2795644
rEBOV-515 Fab	This paper	N/A
rEBOV-442 Fab	Murin et al., 2021	N/A
rEBOV-515 LALA-PG Alexa Fluor 647-labeled	This paper	N/A
rEBOV-442 IgG1 Alexa Fluor 647-labeled	This paper	N/A
MR78 Alexa Fluor 647-labeled	This paper	N/A
Bacterial and virus strains		
Mouse-adapted EBOV /Mayinga (EBOV/M.mus-tc/COD/76/Yambuku-Mayinga, GenBank: AF499101)	Bray et al., 1998	N/A
EBOV-eGFP/Mayinga	Towner et al., 2005	N/A
SUDV strain Gulu (GenBank: AY729654)	Sanchez and Rollin, 2005	N/A
Chimeric EBOV/BDBV-GP-eGFP (GenBank: KU174137)	Ilinykh et al., 2016	N/A
Chimeric EBOV/SUDV-GP-eGFP (GenBank: KU174142)	Ilinykh et al., 2016	N/A
EBOV isolate 199510621 (Kikwit variant)	Cross et al., 2016	N/A
BDBV isolate 200706291 (Uganda variant)	Towner et al., 2008	N/A
SUDV isolate 200011676 (Gulu variant)	Thi et al., 2016	N/A
rVSV/EBOV GP (Mayinga variant)	Garbutt et al., 2004	N/A
rVSV/BDBV GP (Uganda variant)	Mire et al., 2013	N/A
rVSV/SUDV GP (Boniface variant)	Geisbert et al., 2008	N/A
rVSV/EBOV GP and rVSV/BDBV GP viruses that escape neutralization by rEBOV-442, or ADI-15878, or ADI-15946	This paper	N/A
Biological samples		
Human PBMCs	StemCell Technologies	N/A
Chemicals, peptides, and recombinant proteins		
EBOV GP ΔTM (aa 1-636; Makona)	This paper	N/A
BDBV GP ΔTM (aa 1-643; 200706291 Uganda)	This paper	N/A
SUDV GP ΔTM (aa 1-637; Gulu)	This paper	N/A
EBOV/Makona GPΔMuc	Murin et al., 2021	N/A
Thermolysin	Promega	Cat# 9PIV400

(*Continued on next page*)

Continued

REAGENT or RESOURCE	SOURCE	IDENTIFIER
Immobilized papain	ThermoFisher	Cat# 20341
Alexa Fluor 647 NHS ester	ThermoFisher	Cat# A37573
SNAP-Surface Alexa Fluor 647	New England Biolabs	Cat# S9136S
EZ-Link Sulfo-NHS-LC-LC-Biotin	ThermoFisher	Cat# 21338
1-Step Ultra TMB-ELISA	ThermoFisher	Cat# 34029
Freestyle 293 expression medium	ThermoFisher	Cat# 12338002
ExpiCHO Expression Medium	ThermoFisher	Cat# A2910001
Fetal Bovine Serum, ultra-low IgG	ThermoFisher	Cat# 16250078
MabSelect Sure antibody purification resin	Cytiva	Cat# 17543802
Sephadex G-25 medium	Cytiva	Cat# 17-0033-01
Critical commercial assays		
Abbott Piccolo BioChemistry Panel Plus analyzer discs	Fisher Scientific	Cat# 07-P02-15A
Deposited data		
rEBOV-515/rEBOV-442 Fab complex with EBOV GP ΔMucΔTM Makona (cryo-EM)	This paper	PDB:7M8L
rEBOV-515/rEBOV-442 Fab complex with EBOV GP ΔMucΔTM Makona (cryo-EM)	This paper	EMD-23719
Experimental models: cell lines		
Human: Jurkat, clone E6-1	ATCC	ATCC: TIB-152, RRID:CVCL_0367
Human: Jurkat-EBOV GP (Makona)	Gilchuk et al., 2018a; Davis et al., 2019	N/A
Hamster: ExpiCHO-S	ThermoFisher Scientific	Cat# A29127, RRID:CVCL_5J31
Human: FreeStyle 293-F	ThermoFisher Scientific	Cat# R79007, RRID:CVCL_D603
Human: EBOV GPkik-293FS EGFP CCR5-SNAP	J. Lewis	N/A
Monkey: Vero-E6	ATCC	ATCC: CRL-1586, RRID:CVCL_0574
Monkey: Vero	ATCC	ATCC: CCL-81, RRID:CVCL_0059
Experimental models: organisms/strains		
Mouse: BALB/cJ	The Jackson Laboratory	Cat# JAX:000651, RRID:IMSR_JAX:000651
NHP: Macaca mulatta, Chinese origin	PrimGen	N/A
NHP: Macaca fascicularis, Chinese origin	Worldwide Primates	N/A
Recombinant DNA		
Plasmid: EBOV GP ΔTM (aa 1-636; Makona)	Gilchuk et al., 2018a	N/A
Plasmid: BDBV GP ΔTM (aa 1-643; 200706291 Uganda)	Gilchuk et al., 2018a	N/A
Plasmid: SUDV GP ΔTM (aa 1-637; Gulu)	Gilchuk et al., 2018a	N/A
Plasmid: pTwist_rEBOV-515-hG1	This study	N/A
Plasmid: pTwist_rEBOV-515-LALA-PG	This study	N/A
Plasmid: pTwist_rEBOV-442-hG1	This study	N/A
Plasmid: pTwist_rEBOV-442-LALA-PG	This study	N/A
Plasmid: pTwist_ADI-15878-hG1	This paper	N/A
Plasmid: pTwist_ADI-15946-hG1	This paper	N/A
Plasmid: pTwist_2D22-hG1	This paper	N/A
Software and algorithms		
GraphPad Prism 8.4.3	GraphPad Software	GraphPad Prism, RRID:SCR_002798
ForeCyt Standard 6.2 (R1)	Intellicyt	ForeCyt
RTCA version 2.1.0	Agilent Technologies	RTCA Software, RRID:SCR_014821
MotionCorr2	Zheng et al., 2017	MotionCorr2
GCTF	(Zhang, 2016)	GCTF, RRID:SCR_016500
CryoSPARK 2.0	Punjani et al., 2017	CryoSPARK 2.0

(*Continued on next page*)

Continued

REAGENT or RESOURCE	SOURCE	IDENTIFIER
RELION 3.1	Zivanov et al., 2018	RELION, RRID:SCR_016274
UCSF Chimera	Pettersen et al., 2004	UCSF Chimera, RRID:SCR_004097
Phenix	Liebschner et al., 2019	Phenix, RRID:SCR_014224
Rosetta	DiMaio et al., 2015	Rosetta, RRID:SCR_015701
EMRinger	Barad et al., 2015	EMRinger
Coot	Emsley et al., 2010	Coot, RRID:SCR_014222
SWISS-MODEL	Biasini et al., 2014	SWISS-MODEL RRID:SCR_018123
LigPlot	Laskowski and Swindells, 2011	LigPlot
Arpeggio	Jubb et al., 2017	Arpeggio
SynergyFinder 2.0	Ianevski et al., 2020	SynergyFinder
Other		
Piccolo point-of-care analyzer	Abbott	N/A
iQue Screener Plus flow cytometer	Intellicyt	N/A
ÄKTA Pure chromatography system	Cytiva	N/A
Protein Maker	Protein BioSolutions	N/A
Tecnai Spirit electron microscope with TemCam F416 4k x 4k CCD	Zhao et al., 2017	N/A
Synergy H1 microplate reader	BioTek	N/A
Synergy 2 microplate reader	BioTek	N/A
EL406 washer dispenser	BioTek	N/A
Biostack microplate stacker	BioTek	N/A
StrepTrap HP 5 mL column	Cytiva	N/A
HiTrap MabSelect SuRe 5 mL column	Cytiva	Cat# 17-0404-01
xCELLigence RTCA MP analyzer	Agilent Technologies	N/A

RESOURCE AVAILABILITY

Lead contact

Further information and requests for resources and reagents should be directed to and will be fulfilled by the Lead Contact, James E. Crowe, Jr. (james.crowe@vumc.org).

Materials availability

Materials described in this paper are available for distribution under the Uniform Biological Material Transfer Agreement, a master agreement that was developed by the NIH to simplify transfers of biological research materials.

Data and code availability

The EBOV GP ΔMuc ΔTM (Makona)–rEBOV-515–rEBOV-442 Fab cryo-EM structure has been deposited in the PDB with accession code 7M8L. The accession number for the cryo-EM reconstruction reported in this paper have been deposited to the Electron Microscopy Data Bank under accession code EMD-23719 (see Key Resources Table for details). All data needed to evaluate the conclusions in the paper are present in the paper or the Supplemental Information; source data for each of the display items is provided in Key Resources Table.

EXPERIMENTAL MODEL AND SUBJECT DETAILS

Cell lines

Vero-E6 (monkey, female origin) and Vero CCL-81 (monkey, female origin) were obtained from the American Type Culture Collection (ATCC). Vero-E6 cells were cultured in Minimal Essential Medium (MEM) (Thermo Fisher Scientific) supplemented with 10% fetal bovine serum (FBS; HyClone) and 1% penicillin-streptomycin in 5% CO_2, 37°C. Vero CCL-81 cells were cultured in Dulbecco's Modified Eagle Medium (DMEM; Thermo Fisher Scientific)

supplemented with 10% Ultra-Low IgG FBS (GIBCO), 25 mM HEPES, and 100 units/mL of penicillin, and 100 μg/mL of streptomycin (GIBCO) in 5% CO_2, 37°C. A 293F cell line (human, female origin) stably-transfected to express SNAP-tagged EBOV GP

was described previously (Domi et al., 2018). ExpiCHO (hamster, female origin) and FreeStyle 293F (human, female origin) cell lines were purchased from Thermo Fisher Scientific and cultured according to the manufacturer's protocol. The Jurkat-EBOV GP (Makona variant) cell line stably transduced to display EBOV GP on the surface (Davis et al., 2019) was a kind gift from Carl Davis (Emory University, Atlanta, GA). All cell lines were tested on a monthly basis for *Mycoplasma* and found to be negative in all cases.

Viruses

The mouse-adapted EBOV Mayinga variant (EBOV-MA, GenBank: AF49101) (Bray et al., 1998), authentic EBOV Mayinga variant expressing eGFP (Towner et al., 2005), the chimeric infectious EBOV/BDBV-GP (GenBank: KU174137) and EBOV/SUDV-GP (GenBank: KU174142) viruses expressing eGFP (Ilinykh et al., 2016), the infectious vesicular stomatitis viruses rVSV/EBOV GP (Mayinga variant) (Garbutt et al., 2004), rVSV/BDBV GP (Uganda variant) (Mire et al., 2013), or rVSV/SUDV GP (Boniface variant) (Geisbert et al., 2008) expressing an ebolavirus GP that replaces VSV G protein were used for mouse challenge studies or neutralization assays. Viruses were grown and titrated in Vero cell monolayer cultures.

Authentic ebolaviruses EBOV (Cross et al., 2016), BDBV (Towner et al., 2008), and SUDV (Thi et al., 2016) were used for NHP challenge studies. The EBOV isolate 199510621 (Kikwit variant) originated from a 65-year-old female patient who died on 5 May 1995. The study challenge material was from the second Vero-E6 passage of EBOV isolate 199510621. The first passage at UTMB consisted of inoculating CDC 807223 (passage 1 of EBOV isolate 199510621) at a MOI of 0.001 onto Vero E6 cells. SUDV isolate 200011676 (Gulu variant) originated from a 35-year-old male patient who died on 16 October 2000. The study challenge material was from the second Vero-E6 cell passage of SUDV isolate 200011676. The first passage at UTMB consisted of inoculating CDC 808892 (CDC passage 1 of SUDV isolate 200011676) at a MOI of 0.001 onto Vero-E6 cells. BDBV isolate 200706291 (Uganda variant) originated from serum of a patient collected in Uganda on 1 October 2007. The study challenge material was from the second Vero-E6 cell passage of BDBV isolate 200706291 variant Uganda. Briefly, the first passage at UTMB consisted of inoculating CDC 811250 (CDC passage 1 of BDBV isolate 200706291) at a MOI of 0.001 onto Vero-E6 cells. The cell culture fluids were subsequently harvested at day 10 post inoculation with each of indicated viruses and stored at -80°C as $\sim$1 mL aliquots. Neither mycoplasma nor endotoxin were detected ($<$ 0.5 endotoxin units (EU)/mL).

Mouse model

Seven- to eight-week old female BALB/c mice were obtained from the Jackson Laboratory. Mice were housed in microisolator cages and provided food and water *ad libitum*. Challenge studies were conducted under maximum containment in an animal biosafety level 4 (ABSL-4) facility of the Galveston National Laboratory, UTMB. The animal protocols for testing of mAbs in mice were approved by the Institutional Animal Care and Use Committee of the University of Texas Medical Branch (UTMB) in compliance with the Animal Welfare Act and other applicable federal statutes and regulations relating to animals and experiments involving animals.

Nonhuman primate (NHP) model

Three- to four-year-old male (n = 6) or female (n = 6) rhesus macaques used in this study were obtained from PrimGen. Four-year-old male (n = 3) or female (n = 3) cynomolgus monkeys were obtained from Worldwide Primates. NHP research adhered to principles stated in the eighth edition of the Guide for the Care and Use of Laboratory Animals . The facility where this research was conducted [University of Texas Medical Branch (UTMB)] is fully accredited by the Association for Assessment and Accreditation of Laboratory Animal Care International and has an approved Office of Laboratory Animal Welfare Assurance (#A3314-01).

METHOD DETAILS

Monoclonal antibody production and purification

Sequences of monoclonal antibodies that had been synthesized as cDNA (Twist Bioscience) and cloned into an IgG1 or IgG1 LALA-PG monocistronic expression vector (designated as pTwist-mCis_G1 or pTwist-mCis_hG1 LALA-PG) were used for monoclonal antibody secretion in mammalian cell culture. This vector contains an enhanced 2A sequence and GSG linker that allows the simultaneous expression of monoclonal antibody heavy and light chain genes from a single construct upon transfection (Chng et al., 2015). CHO cell cultures were transfected using the GIBCO ExpiCHO Expression System protocols as described by the vendor. Culture supernatants were purified using 5 mL HiTrap MabSelect SuRe (Cytiva, formerly GE Healthcare Life Sciences) column and an ÄKTA pure chromatography system (Cytiva). Purified monoclonal antibodies were buffer-exchanged into PBS, concentrated using Amicon Ultra-4 50-kDa centrifugal filter units (Millipore Sigma) and stored at 4 $^{\circ}$C until use. For NHP treatment studies antibodies were purified from 5 to 15 L of CHO supernatant using HiScale 26/20 column (Cytiva) packed with MabSelect SuRe resin, purified protein was buffer-exchanged into PBS using HiScale 50/40 column packed with Sephadex G-25 (medium) resin (GE Healthcare Life Sciences), concentrated, and stored at -80 $^{\circ}$C until use. Purified monoclonal antibodies were tested routinely for endotoxin levels (found to be less than 30 EU per mg IgG for mouse studies and less than 1 EU per mg IgG for NHP studies). Endotoxin testing was performed using the PTS201F cartridge (Charles River), with a sensitivity range from 10 to 0.1 EU per mL, and an Endosafe Nexgen-MCS instrument (Charles River). For structural studies, Fab was produced after co-transfection of ExpiCHO cells with two separate mammalian expression vectors containing antibody light chain and Fab heavy chain sequences as described

previously (Gilchuk et al., 2020b). Fab proteins were purified using CaptureSelect column (Thermo Fisher Scientific). Purified antibodies were buffer-exchanged into PBS, concentrated using Amicon Ultra-4 30 kDa MWCO centrifugal filter units (Millipore Sigma) and stored at 4°C until use.

GP expression and purification

For ELISA studies, the ectodomains of EBOV GP ΔTM (residues 1-636; strain Makona; GenBank: KM233070), BDBV GP ΔTM (residues 1-643; strain 200706291 Uganda; GenBank: NC_014373), and SUDV GP ΔTM (residues 1-637; strain Gulu; GenBank: NC_006432) were expressed and purified as described before (Gilchuk et al., 2018a). For structural studies, the ectodomain of EBOV/Makona GP (residues 32-644, GenBank AKG65268.1) lacking residues 310-460 of the mucin-like domain to produce EBOV/Makona GPΔMuc was produced and purified as described before (Murin et al., 2021).

ELISA binding assay

To assess mAb binding at different pH, wells of 96-well microtiter plates were coated with purified, recombinant EBOV, BDBV or SUDV GPΔTM ectodomains at 4°C overnight. Plates were blocked with 2% non-fat dry milk and 2% normal goat serum in DPBS containing 0.05% Tween-20 (DPBS-T) for 1 h. Purified mAbs were diluted serially in DPBS-T (pH 7.4), or DPBS-T that was adjusted to pH 5.5 or 4.5 with hydrochloric acid, added to the wells and incubated for 1 h at ambient temperature. The bound antibodies were detected using goat anti-human IgG conjugated with horseradish peroxidase (Southern Biotech) diluted in blocking buffer. Color development was monitored using TMB (3,3′,5,5′-tetramethylbenzidine) substrate (Thermo Fisher Scientific), 1N hydrochloric acid was added to stop the reaction, and the absorbance was measured at 450 nm using a spectrophotometer (Biotek).

Mammalian cell-surface-displayed GP antibody binding

Binding of Alexa Fluor 647-labeled antibody to Jurkat-EBOV GP cell line was assessed by flow cytometry using an iQue Screener Plus high throughput flow cytometer (Intellicyt) as we described previously (Gilchuk et al., 2020b).

Measurement of synergistic GP binding by a combination of antibodies

Serially-diluted Alexa Fluor 647-labeled antibody rEBOV-442 IgG1 or rEBOV-515 LALA-PG was titrated into serially-diluted unlabeled partner antibody to generate a pairwise combinatorial matrix of two antibodies in the mixture. For antibody dilutions and washes, we used DPBS (Dulbecco's phosphate-buffered saline) containing 2% of heat-inactivated FBS and 2 mM EDTA (ethylenediaminetetraacetic acid, sodium salt) (pH 8.0) designated as incubation buffer. For antibody staining, ~5×10^4 Jurkat EBOV-GP cells were added per each well of V-bottom 96-well plate (Corning) in 5 μL of the incubation buffer, and antibody mixtures were added to the cells in duplicate for total volume of 50 μL per well, followed by 2 hr incubation at 4°C. Cells were washed with the incubation buffer by centrifugation at 400 x *g* for 5 min at ambient temperature and binding to the GP was assessed using iQue Screener Plus flow cytometer. Data for up to 5,000 events per well were acquired, and data were analyzed with ForeCyt (Intellicyt) software. Dead cells were excluded from the analysis on the basis of forward and side scatter gate for viable cell population. Binding was calculated as the percent of the maximal median fluorescence intensity signal (MFI) by the highest concentration of respective fluorescently-labeled antibody alone (25 μg/mL). Synergy distribution maps were generated from the dose-response binding matrix using a web application, SynergyFinder 2.0, and data were analyzed using ZIP synergy scoring model (Ianevski et al., 2020).

Selection and sequencing of VSV/EBOV GP mutants that escape antibody neutralization

To screen for escape mutations selected in the presence of individual antibodies or antibody cocktails, we used a real-time cell analysis (RTCA) assay and xCELLigence RTCA MP Analyzer (ACEA Biosciences) with modification of recently described assays (Gilchuk et al., 2020a; Greaney et al., 2021). Fifty (50) μL of cell culture medium (DMEM supplemented with 2% FBS) was added to each well of a 96-well E-plate to obtain a background reading. Eighteen thousand (18,000) Vero cells in 50 μL of cell culture medium were seeded per each well, and plates were placed on the analyzer. Measurements were taken automatically every 15 min and the sensograms were visualized using RTCA software version 2.1.0 (ACEA Biosciences Inc). VSV/EBOV GP virus (20,000 plaque forming units [PFU] per well, ~1 MOI) was mixed with a saturating neutralizing concentration of individual antibody (10 μg/mL) or two-antibody cocktail (1:1 antibody ratio, 10 μg/mL total antibody concentration) in a total volume of 100 μL and incubated for 1 h at 37°C. At 16-20 h after seeding the cells, the virus-antibody mixtures were added into 8 to 96 replicate wells of 96-well E-plates with cell monolayers. Wells containing only virus in the absence of antibody and wells containing only Vero cells in medium were included on each plate as controls. Plates were measured continuously (every 15 min) for 72 h. The escape mutants were identified by delayed CPE in wells containing antibody. To verify escape from antibody selection, isolated viruses were assessed in a subsequent RTCA experiment in the presence of 20 μg/mL of antibody used for the escape selection, or 20 μg/mL of the other tested individual mAbs (rEBOV-442, rEBOV-515, ADI-15878, or ADI-15946), or 20 μg/mL of 1:1 cocktail of rEBOV-442+rEBOV-515 (see Figure S1C).

To verify the escape phenotype mediated by mutations present in GP protein-expressing VSV antibody-selected escape variants, the escape viruses isolated after RTCA escape screening were propagated in 6-well culture plates with confluent Vero cells in the presence of 20 μg/mL of mAb used. Viral RNA was isolated using a QiAmp Viral RNA extraction kit (QIAGEN) from aliquots of supernatant containing a suspension of the selected virus population. The GP protein gene cDNA was amplified with a SuperScript IV One-Step RT-PCR kit (Thermo Fisher Scientific) using primers flanking the GP gene. The amplified PCR product (~2,400 bp) was

purified using SPRI magnetic beads (Beckman Coulter) at a 1:1 ratio and sequenced by the Sanger sequence technique using primers giving forward and reverse reads of the glycan cap region of the GP.

Neutralization assays

BSL-4 virus neutralization assays were performed using recombinant EBOV-eGFP or chimeric EBOV viruses in which GP was replaced with its counterpart from BDBV or SUDV, as described previously (Ilinykh et al., 2016). Briefly, four-fold dilutions of the respective mAb starting at 200 μg/mL were mixed in triplicate with 400 PFU of the virus in U-bottom 96-well plates and incubated for 1 hr at 37°C. Mixtures were applied on Vero-E6 cell monolayer cultures in 96-well plates and incubated for four days at 37°C. In the absence of mAb neutralizing activity, the infection resulted in uniform eGFP fluorescence from the monolayer of cells that was detected readily by fluorescence microscopy. Fluorescence was measured using Synergy HT microplate reader (BioTek). Half maximal inhibitory concentration (IC_{50}) values were determined by nonlinear regression analysis using Prism software.

BSL-2 virus neutralization experiments were performed using the infectious rVSV/EBOV GP, rVSV/BDBV GP, and rVSV/SUDV GP viruses, and we adopted high-throughput RTCA assay that quantify virus-induced cytopathic effect (CPE) (Gilchuk et al., 2020a, 2020b). Viruses were pre-titrated by RTCA to determine dilution of each virus stock to achieve similar CPE kinetics and complete CPE in 32 h after applying virus alone to Vero cells. Fifty (50) μL of cell culture medium (DMEM supplemented with 2% FBS) was added to each well of a 96-well E-plate using a ViaFlo384 liquid handler (Integra Biosciences) to obtain background reading. Eighteen thousand (18,000) Vero cells in 50 μL of cell culture medium were seeded per each well, and the plate was placed on the analyzer. Measurements were taken automatically every 15 min, and the sensograms were visualized using RTCA software version 2.1.0 (ACEA Biosciences Inc). VSV/EBOV GP (~0.1 MOI, ~2,000 PFU per well), or VSV/BDBV GP (0.04 MOI, ~800 PFU per well) or VSV/SUDV GP (0.01 MOI, ~240 PFU per well) were mixed 1:1 with respective dilution of mAb in triplicate a total volume of 100 μL using DMEM supplemented with 2% FBS as a diluent and incubated for 1 h at 37°C in 5% CO_2. At 16 to 18 h after seeding the cells, the virus-mAb mixtures were added to the cells in 96-well E-plates. Triplicate wells containing virus only (maximal CPE in the absence of mAb) and wells containing only Vero cells in medium (no-CPE wells) were included as controls. Plates were measured continuously (every 15 min) for 48 h to assess virus neutralization. Normalized cellular index (CI) values at the endpoint (42 h after incubation with the virus) were determined using the RTCA software version 2.1.0 (ACEA Biosciences). Results were expressed as percent neutralization in the presence of a particular mAb relative to no-CPE control wells minus CI values from control wells with maximum CPE. RTCA IC_{50} values were determined by nonlinear regression analysis using Prism software.

Measurement of synergistic virus neutralization by a combination of antibodies

We used RTCA assay to assess neutralizing activity from a pairwise combinatorial matrix of two antibodies in the mixture. Serially-diluted rEBOV-442 (2-fold dilutions) was titrated into serially-diluted rEBOV-515 (two-fold dilutions) and incubated with rVSV/EBOV GP, rVSV/BDBV GP, or rVSV/SUDV GP viruses for 1 h at 37°C. Virus-antibody mixtures were applied to Vero cells grown in 96-well E-plates in duplicates for each virus and using separate plates for each pairwise combinatorial matrix. Triplicate wells containing virus only (maximal CPE in the absence of mAb) and wells containing only Vero cells in medium (no CPE wells) were included as controls. Plates were measured continuously (every 15 min) for 48 h to assess virus neutralization. Normalized cellular index (CI) values at the endpoint (42 h after incubation with the virus) were determined using the RTCA software version 2.1.0 (ACEA Biosciences). Results were expressed as percent neutralization in the presence of a particular mAb relative to control wells with no CPE minus CI values from control wells with maximum CPE. Synergy distribution maps were generated from the dose-response binding matrix using a web application, SynergyFinder 2.0, and data were analyzed using ZIP synergy scoring model (Ianevski et al., 2020).

Rapid fluorometric antibody-mediated cytotoxicity assay (RFADCC)

Antibody-dependent cell-mediated cytotoxicity activity of EBOV GP-reactive IgG was quantified with an EBOV-adapted modification of the RFADCC assay (Domi et al., 2018; Orlandi et al., 2016). Briefly, a target cell line was made by transfecting 293F cells with a full-length DNA expressing GP from the EBOV (Kikwit variant) followed by transfecting with two separate DNA constructs expressing eGFP and the chimeric CCR5-SNAP tag protein. The new cell line, designated EBOV GPkik-293FS eGFP CCR5-SNAP, expresses EBOV-Kikwit GP on the plasma membrane, eGFP in the cytoplasm and the SNAP-tag CCR5, which can be specifically labeled with SNAP-Surface Alexa Fluor 647 (New England Biolabs), on the cell surface (Domi et al., 2018). The unrelated human mAb DENV 2D22 and the Fc effector function disabled mAb rEBOV-515 LALA-PG were used as negative controls for the assay background. The ADCC activity was quantified by incubating three-fold serial dilutions of mAbs with EBOV GPkik-293FS eGFP CCR5-SNAP target cells for 15 min at ambient temperature and then adding human PBMC (STEMCELL Technologies) as effector cells for 2 hr at 37°C, after which cells were washed once with PBS, fixed with 2% paraformaldehyde, stained and analyzed using an iQue Screener Plus flow cytometer (Intellicyt). Data analysis was performed with ForeCyt (Intellicyt) software. The percentage cytotoxicity of the mAb was determined as the number of target cells losing eGFP signal (by virtue of ADCC) but retaining the surface expression of CCR5-SNAP.

GP cleavage inhibition

The assay was performed as we described previously (Gilchuk et al., 2018a). Briefly, Jurkat-EBOV GP cells were pre-incubated with serial dilutions of mAbs in DPBS for 20 min at room temperature, then incubated with thermolysin (Promega) diluted in DPBS

to 1 mg/mL for 20 min at 37°C. The reaction was stopped by addition of the incubation buffer containing DPBS, 2% heat-inactivated FBS and 2 mM EDTA (pH 8.0). Washed cells were incubated with 5 μg/mL of Alexa Fluor 647-labeled EBOV GP RBD-reactive mAb MR78 (Bornholdt et al., 2016) at 4°C for 60 min. Stained cells were washed, fixed, and analyzed by flow cytometry using Intellicyt iQue. Cells were gated for the viable population, and median fluorescence intensity from Alexa Fluor 647 was determined. Background staining was determined from binding of the labeled mAb MR78 to Jurkat-EBOV GP (uncleaved) cells. Results are expressed as the percent of RBS exposure inhibition in the presence of tested mAb relative to controls for minimal binding of labeled MR78 mAb-only to intact (uncleaved) Jurkat EBOV-GP, and maximal binding of labeled MR78 mAb-only to cleaved Jurkat-EBOV GP.

Mouse challenge

Groups of mice (n = 5 per group) were inoculated with 1,000 PFU of the EBOV-MA by the intraperitoneal (i.p.) route. Mice were treated i.p. with indicated doses of individual mAbs on 1 day after virus inoculation (dpi). Human mAb DENV 2D22 served as a control. Mice were monitored twice daily from 0 to 14 dpi for illness, survival, and weight loss, followed by once daily monitoring from 15 dpi to the end of the study at 28 dpi. The extent of disease was scored using the following parameters: score 1 – healthy; score 2 – ruffled fur and hunched posture; score 3 – a score of 2 plus one additional clinical sign such as orbital tightening and/or >15% weight loss; score 4 – a score of 3 plus one additional clinical sign such as reluctance to move when stimulated, or any neurologic signs (seizures, tremors, head tilt, paralysis, etc.), or >20% weight loss. Animals reaching a score of 4 were euthanized as per the IACUC-approved protocol. All mice were euthanized on day 28 after EBOV challenge.

NHP challenge

Twelve healthy adult rhesus macaques (*Macaca mulatta*) of Chinese origin and six healthy adult cynomolgus monkeys (*Macaca fascicularis*) were studied. Animals were assigned to three groups of five animals per treatment group and a control untreated animal. Animals were randomized by random number assignment (with Microsoft Excel) into a treatment group and a control animal. Previous studies showed a difference of the disease courses between EBOV, BDBV, or SUDV challenged NHP models of EVD (Bornholdt et al., 2019; Gilchuk et al., 2020b; Herbert et al., 2020). EBOV causes rapid infection with readily detectable systemic viremia by 3 dpi. In the SUDV challenge model, the disease course is slower than that caused by EBOV, and the disease course caused by BDBV is even slower than those of EBOV or SUDV. Given these differences, the first antibody treatment in each model was delivered at the earliest time points after viral challenge at which animals are expected to be uniformly viremic (*e.g.*, day 3 after EBOV, day 4 after SUDV, or day 6 after BDBV challenge). The treatment schedule using a two-dose 30 mg/kg/dose regimen given 3 days apart was the same as in our previous work in which we tested a different cocktail of mAbs (rEBOV-520 LALA + rEBOV-548 IgG) in NHPs against EBOV only (Gilchuk et al., 2020b) to allow comparisons between two studies. After intramuscular challenge with a lethal target dose of 1,000 plaque-forming units (PFU) of EBOV/Kikwit, BDBV/Uganda, or SUDV/Gulu, each of the NHPs of the treatment group received intravenously two 30 mg/kg doses of the cocktail (a 2:1 mixture of rEBOV-515 LALA-PG and rEBOV-442 IgG1) spaced 3 days apart (days 3 and 6 after EBOV/Kikwit, days 6 and 9 after BDBV/Uganda, or days 4 and 7 after SUDV/Gulu inoculation). The back-titer of the EBOV, BDBV, and SUDV inoculum identified 963, 1113, and 988 PFU as the actual inoculation dose for the respective virus. Historical untreated controls for EBOV challenge cohort included fourteen untreated animals from separate studies including 11 animals, as we reported previously (Gilchuk et al., 2020b), which were challenged with the same target dose of EBOV/Kikwit and by the same route. Historical untreated controls for SUDV/Gulu challenge cohort included five untreated animals from previous study (Thi et al., 2016) and four untreated animals from two other studies (T.W.G. and R.W.C., unpublished data) that were challenged with the same target dose of BDBV and by the same route. Historical untreated controls for BDBV challenge cohort included three untreated animals from a previous study (Bornholdt et al., 2019) and seventeen untreated animals from the other studies (T.W.G. and R.W.C., unpublished data) that were challenged with the same target dose of BDBV/Uganda and by the same route. All animals were given physical exams, and blood was collected at the time of inoculation and at indicated times after virus inoculation. In addition, all animals were monitored daily and scored for disease progression with an internal filovirus scoring protocol approved by the UTMB Institutional Animal Care and Use Committee. The scoring measured from baseline and included posture or activity level, attitude or behavior, food and water intake, respiration, and disease manifestations such as visible rash, hemorrhage, ecchymosis, or flushed skin. A score of $\geq$ 9 indicated that an animal met criteria for euthanasia. These studies were not blinded, and all animals were included in analysis.

Measurement of virus load in NHP blood and tissues

Titration of virus in plasma samples and 10% tissue homogenates (w/v) was performed by plaque assay in Vero-E6 cell culture monolayers. Briefly, serial 10-fold dilutions of the samples were applied to Vero-E6 cell monolayers in duplicate wells (200 μL); the limit of detection was 25 PFU/mL for plasma and 250 PFU/gram for tissue. For qRT-PCR analysis, RNA was isolated from whole blood or tissue using the Viral RNA Mini-kit (QIAGEN) using 100 μL of blood or 100 mg of tissue into 600 μL of buffer AVL. Primers (probes) targeting the VP30 gene of EBOV probe sequence of 6-carboxyflourescein (6FAM)-5′ CCG TCA ATC AAG GAG CGC CTC 3′-6 carboxytetramethylrhodamine (TAMRA) (Thermo Fisher Scientific), the VP35 intergenic region of BDBV probe sequence of 6FAM-5′ CGCAACCTCCACAGTCGCCT 3′-TAMRA, and the L gene of SUDV probe sequence of 6FAM-5′ CAT CCA ATC AAA GAC ATT GCG A 3′-TAMRA were used for qRT-PCR. EBOV RNA was detected using the CFX96 detection system (BioRad Laboratories) in One-step probe qRT-PCR kits (QIAGEN) with the following cycle conditions: 50°C for 10 min, 95°C for 10 s, and 40 cycles of

95°C for 10 s and 57°C for 30 s for EBOV and BDBV and 50°C for 10 min, 95°C for 10 s, and 40 cycles of 95°C for 10 s and 59°C for 30 s for SUDV. Threshold cycle (CT) values representing EBOV, BDBV and SUDV genomes were analyzed with CFX Manager Software, and data are depicted as genome equivalents (GEq); the limit of detection was 3.7 $\log_{10}$GEq/mL for blood and 3.7 $\log_{10}$GEq/g for the tissues.

NHP serum biochemistry

Serum samples collected from NHPs were tested for concentrations of albumin, amylase, alanine aminotransferase, aspartate aminotransferase, alkaline phosphatase, gamma-glutamyltransferase, glucose, blood urea nitrogen, creatinine, total protein, and C-reactive protein by using a Piccolo point-of-care analyzer and Abbott Piccolo BioChemistry Panel Plus analyzer discs (Fisher Scientific).

Sample preparation for cryogenic electron microscopy

EBOV/Makona GPΔmuc was incubated overnight with a 5-fold molar excess of rEBOV-515 Fab, rEBOV-442 Fab, and rADI-16061 Fab at 4°C. The complexes were then purified by SEC using an S200I column equilibrated in 1X TBS and concentrated to 5 mg/mL using a 100-kDa concentrator (Amicon Ultra, Millipore). Immediately prior to freezing, 0.06 mM of n-Dodecyl β-D-maltoside (Anatrace) was added to 3 μL of the complex. Vitrification was performed with a Vitrobot (Thermo Fisher Scientific) equilibrated to 4°C and 100% humidity. Cryo-EM grids were plasma cleaned for 5 s using a mixture of Ar/O2 (Gatan Solarus 950 Plasma system) followed by blotting on both sides of the grid with filter paper (Whattman No. 1). See Table S7 for additional details. Note that ADI-16061 Fab was added to assist in angular sampling and orientations of the complexes in ice as we described previously (Gilchuk et al., 2020b).

Cryogenic electron microscopy data collection and processing

Cryo-EM data were collected according to Table S7. Micrographs were aligned and dose-weighted using MotionCor2 (Zheng et al., 2017). CTF estimation was completed using GCTF (Zheng et al., 2017). Particle picking and initial 2D classification were initially performed using CryoSPARC 2.0 (Punjani et al., 2017) to clean up particle stacks and exclude any complexes that were degrading. Particle picks were then imported into Relion 3.1 (Zivanov et al., 2018) for 3D classification and refinement using C3 symmetry and a tight mask around the GP/rEBOV-515 Fab/rEBOV-442 Fab complex. CTF refinement was then performed by either Relion or Cryosparc to increase map quality and resolution. There was no electron density for ADI-16061 Fab.

Cryogenic electron microscopy model building and refinement

Homology models of Fab were first generated using SWISS-MODEL (Biasini et al., 2014). A model of EBOV GP (PDB: 5JQ3) was then added to generate a starting model used for refinement. The starting model was fit into the cryo-EM map using UCSF Chimera (Pettersen et al., 2004) and refined initially using Phenix real-space refinement (Liebschner et al., 2019). The refined model was then used as a starting model for relaxed refinement in Rosetta (DiMaio et al., 2015). The top five models then were evaluated for fit in EM density and adjusted manually using Coot (Emsley et al., 2010) to maximize fit. Finally, Man9 glycans were fit into glycan densities, trimmed and then a final refinement was performed in Rosetta. The final structures were evaluated using EMRinger (Barad et al., 2015) and Molprobity from Phenix. Glycans were validated using Privateer (Agirre et al., 2015) and PDBcare (Lütteke and von der Lieth, 2004). All map and model images were generated in UCSF Chimera (Pettersen et al., 2004). Antibody contacts were analyzed using LigPlot (Laskowski and Swindells, 2011), Arpeggio (Jubb et al., 2017) and UCSF Chimera (Pettersen et al., 2004).

QUANTIFICATION AND STATISTICAL ANALYSIS

The descriptive statistics mean ± SEM or mean ± SD were determined for continuous variables as noted. Survival curves were estimated using the Kaplan-Meier method and overall difference in survival between the groups in mouse studies was estimated using two-sided log rank test (Mantel-Cox) with subjects right censored, if they survived until the end of the study. In NHP studies, survival curves were estimated using the Kaplan-Meier method, and the proportion surviving at day 28 after virus inoculation was compared using a 2-sided exact unconditional test of homogeneity. Curves for antibody binding were fitted after log transformation of antibody concentrations using a four-parameter log-logistic (4PL) analysis. In neutralization assays and GP cleavage inhibition assays, IC_{50} values were calculated after log transformation of antibody concentrations using a four-parameter log-logistic (4PL) analysis. Synergy distribution maps were generated from the dose-response binding matrix using an open-source software SynergyFinder 2.0: visual analytics of multi-drug combination synergies (https://synergyfinder.fimm.fi), and data were analyzed using ZIP synergy scoring model (Ianevski et al., 2020). Technical and biological replicates are indicated in the figure legends. Statistical analyses were performed using Prism v8.4.3 (GraphPad).

Supplemental figures

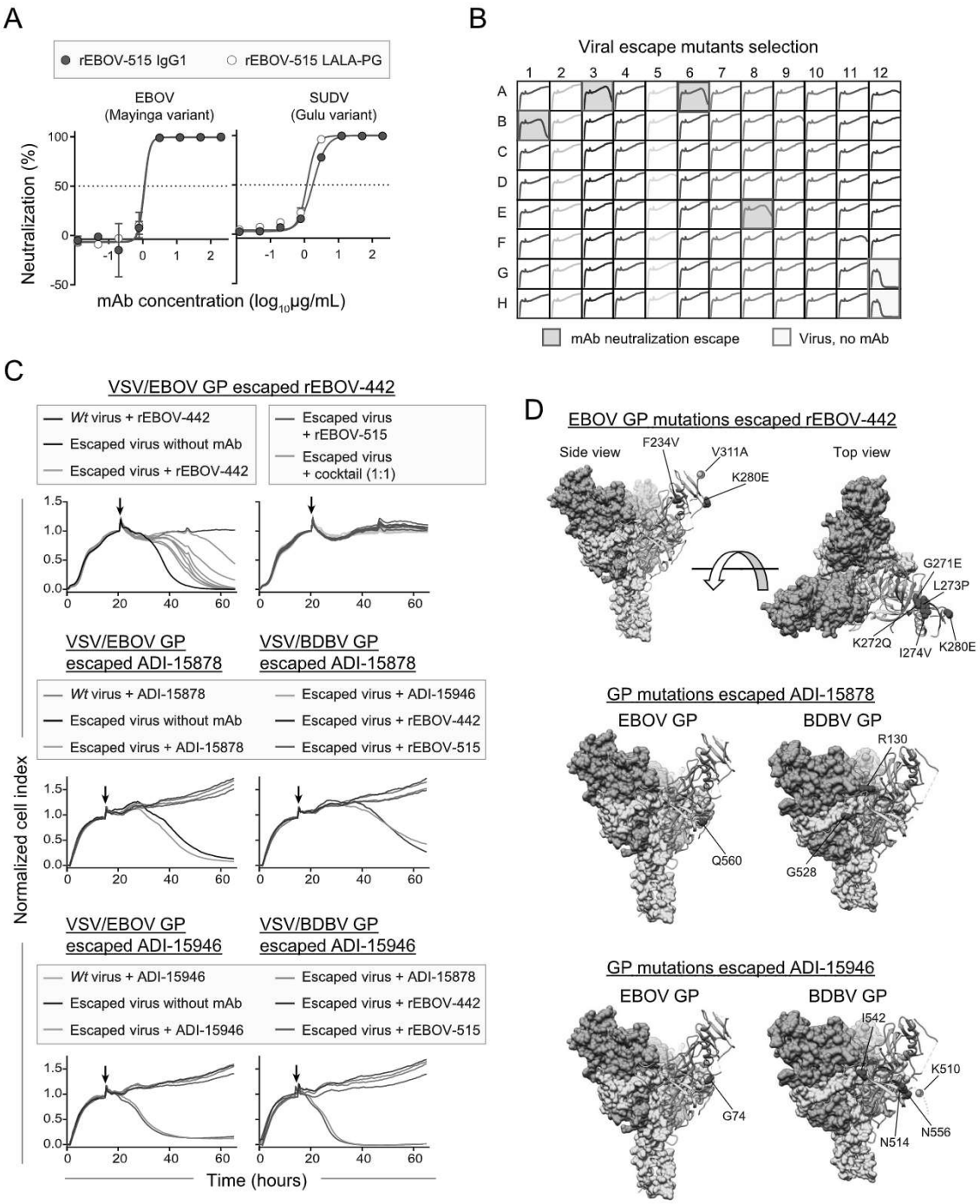

Figure S1. Neutralizing activity of antibody rEBOV-515 LALA-PG and mutations in the GP for the individual broadly-neutralizing mAbs rEBOV-442, rEBOV-515, ADI-15878, and ADI-15946, related to Figure 1

(A) EBOV or SUDV neutralization by wild-type IgG1 or IgG1 LALA-PG variants of rEBOV-515. Neutralization was assessed with chimeric ebolaviruses encoding EBOV or SUDV GP as in Figure 1A. Mean ± SD of technical triplicates from one experiment are shown.

(B) Example RTCA sensograms from individual wells of 96-well E-plate analysis showing VSV/EBOV GP viruses that escaped neutralization (shown with overlayed semi-transparent blue boxes) by mAb ADI-15878 after the first passage. Escape in the illustrated wells was confirmed using a second-passage study and then validated as in (C).

(legend continued on next page)

(C) RTCA sensograms for neutralization of mAbrEBOV-442-, ADI-15878-, or ADI-15946-selected escape viruses by individual mAbs rEBOV-442, rEBOV-515, ADI-15878, or ADI-15946, or a 1:1 cocktail of rEBOV-442 + rEBOV-515 (defined as the "cocktail"). The escape selection was performed using infectious chimeric VSV expressing EBOV or BDBV GP as in Figure 1D. Seven viruses that escaped neutralization by rEBOV-442 and had sequence-verified mutations in the gene encoding the glycan cap region of the GP, and one representative virus that escaped neutralization by ADI-15878 or ADI-15946 with sequence-verified mutations in the GP were incubated in the presence of a saturating concentration (20 μg/mL) of mAb used for the escape selection (shown in gray), or other indicated mAbs (see color code keys in the figure), or the cocktail (green). Cytopathic effect (CPE) was monitored kinetically in Vero cells after applying the virus-mAb mixtures to the cells. Sensograms for CPE by the wild-type chimeric VSV/EBOV GP or VSV/BDBV GP without mAb (black), and full neutralization of the wild-type virus by individual mAbs are shown as the controls. All sequence-verified escape mutations for the viruses selected by rEBOV-442, ADI-15878, and ADI-15946 are indicated in Figure 1D.

(D) Mutations in indicated residues (magenta) identified in the EBOV GP (PDB: 5JQ3) or BDBV GP (PDB: 6DZM) lacking mucin-like domains for the selected viruses that escaped neutralization by rEBOV-442 (top), ADI-15878 (middle), or ADI-15946 (bottom) as in (C). Positions of V311 and K510 residues that are not present in the crystal or cryo-EM GP structure and are shown with gray spheres with magenta center.

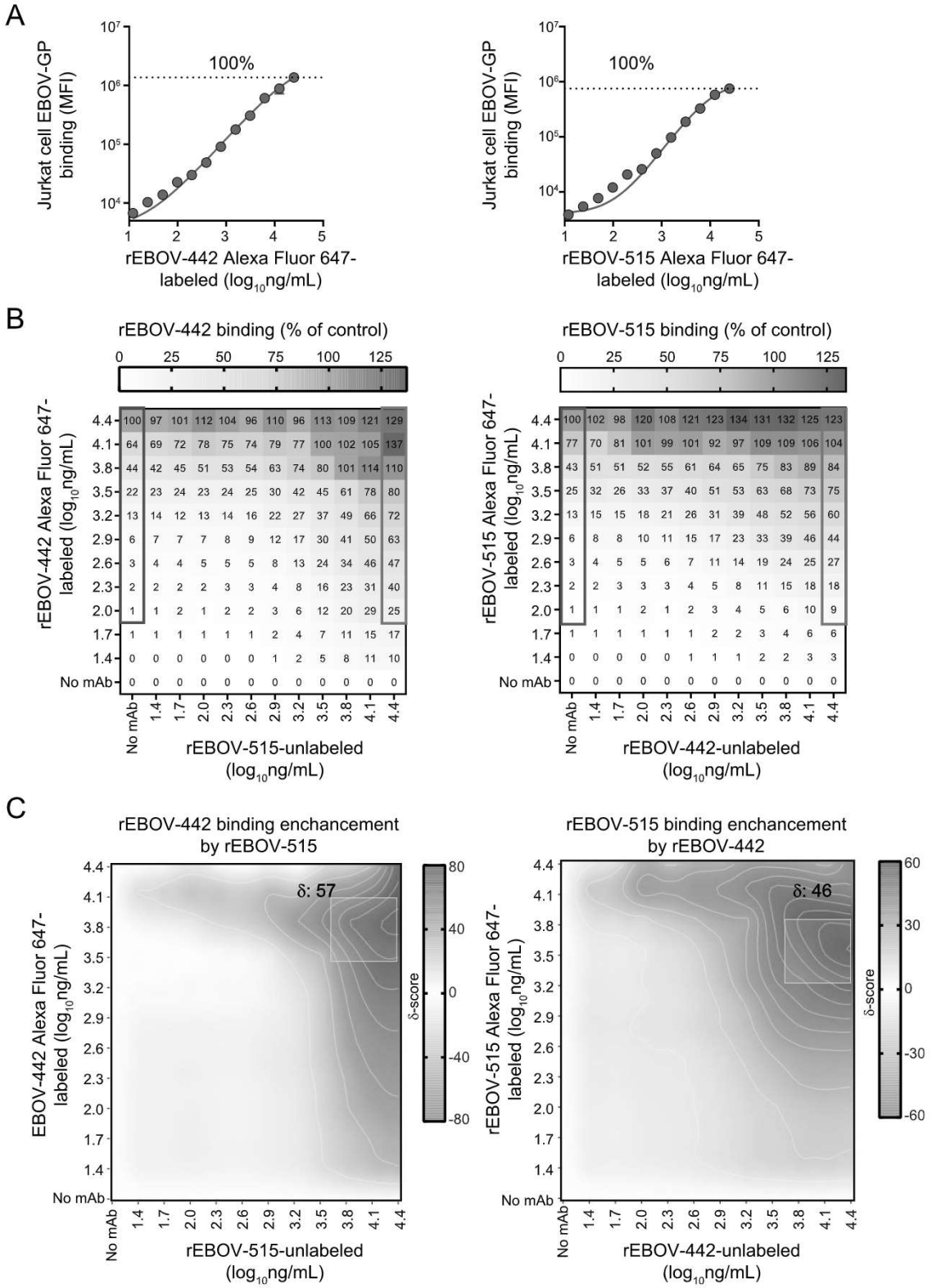

Figure S2. Reciprocal synergistic binding activity in the cocktail of rEBOV-442 and rEBOV-515, related to Figure 3

Serially-diluted Alexa Fluor 647-labeled mAb rEBOV-442 IgG1 or rEBOV-515 LALA-PG was titrated into serially-diluted unlabeled partner mAb to generate a pairwise combinatorial matrix of two mAbs in the mixture. Binding to Jurkat EBOV-GP cells was assessed by flow cytometric analysis.

(legend continued on next page)

(A) Dose-response binding of fluorescently-labeled rEBOV-442 alone (left) or rEBOV-515 alone (right) to Jurkat-EBOV GP. Mean ± SD of technical duplicates is shown.

(B) Binding dose-response matrix by rEBOV-442 or rEBOV-515 bound to the EBOV-GP in the presence of a partner mAb. Axes denote the concentration of each mAb, with the percent binding shown in each square. Binding was calculated as the percent of the maximal median fluorescence intensity signal (MFI) by the highest concentration of respective fluorescently-labeled mAb alone (25 μg/mL) as in (A). Examples of an enhanced binding activity by a combination of fluorescently-labeled mAb plus partner mAb at the highest tested concentration (green box) in a comparison to the binding by fluorescently-labeled rEBOV-442 alone (violet box) or rEBOV-515 alone (raspberry box) are shown.

(C) Synergy distribution map generated from the dose-response binding matrix in (B). Red color indicates areas in which synergistic neutralization was observed; shaded gray box indicates the area of maximum synergy between the two monoclonal antibodies, and δ-score for this area is shown. δ-score is a synergy score: a value of −10 indicates antagonism; a value of −10 to 10 indicates an additive effect; a value of > 10 indicates synergy. Data in (A-B) are from a representative experiment performed in technical duplicate and repeated twice.

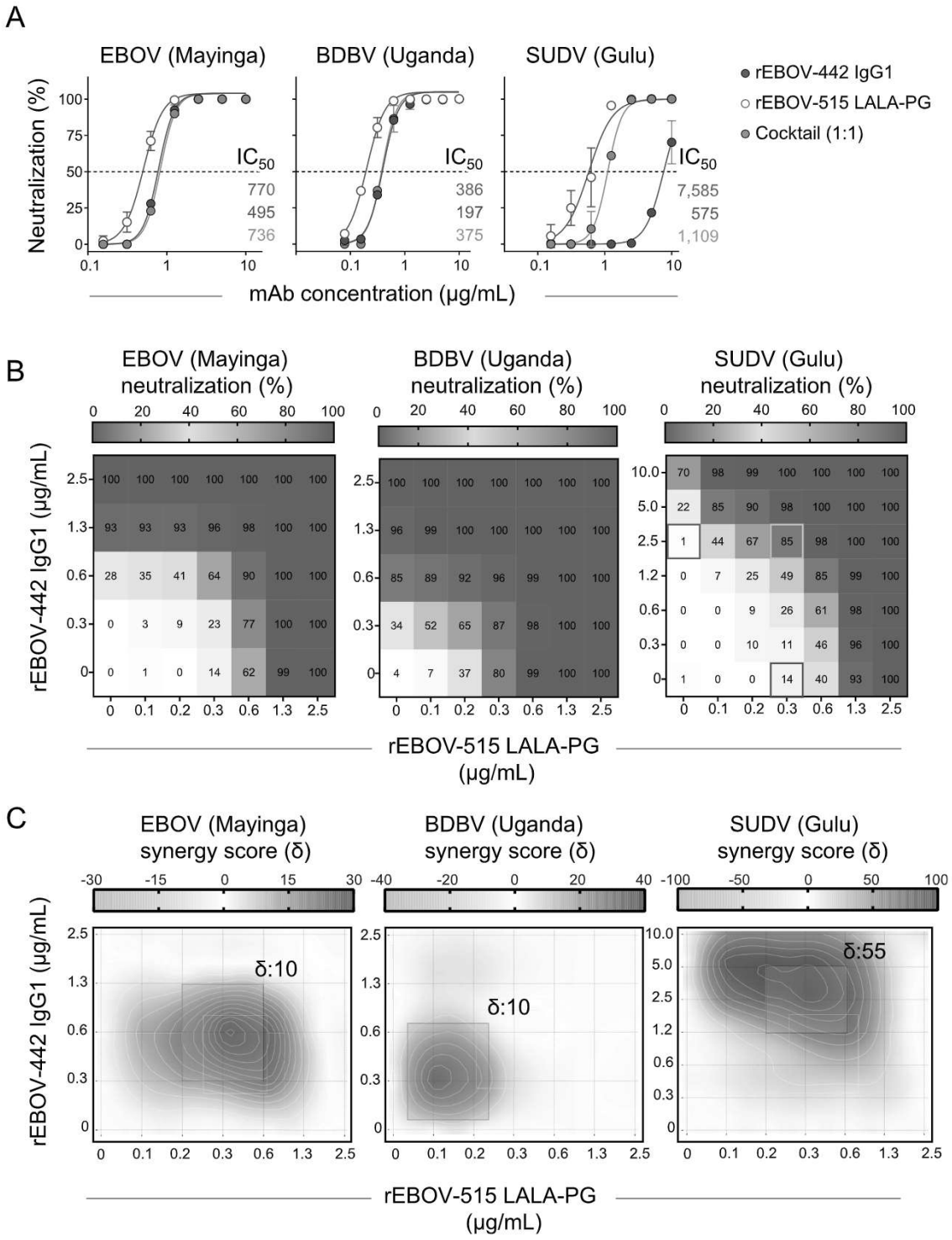

Figure S3. Broad and synergistic neutralizing activity mediated by the cocktail of rEBOV-442 and rEBOV-515, related to Figure 3

Neutralizing activity of individual antibodies or their mixture was assessed using chimeric ebolaviruses encoding EBOV (Mayinga variant), BDBV (Uganda variant), or SUDV (Gulu variant) GP as in Figure 1A.

(A) Neutralization of EBOV, BDBV, or SUDV by rEBOV-442 alone, rEBOV-515 alone, or a 1:1 mixture of rEBOV-442 and rEBOV-515. Mean ± SD of technical duplicates is shown.

(B) Serially-diluted rEBOV-442 was titrated into serially-diluted rEBOV-515 to generate a pairwise combinatorial matrix of two antibodies in the mixture. The matrix shows neutralization dose-response data for EBOV, BDBV, or SUDV, by indicated concentrations of rEBOV-442 and rEBOV-515. Axes denote the concentration

(legend continued on next page)

of each mAb, with the percent neutralization shown in each square. The heatmap denotes a gradient of 0 (white) to 100% (red) neutralization. Examples of synergistic SUDV neutralization by rEBOV-515 alone (raspberry box) or rEBOV-442 alone (blue box) in comparison to a combined indicated concentration of two mAbs in the cocktail (green box) are shown.

(C) Synergy distribution map generated from the dose-response neutralization matrix in (B). Red color indicates areas in which synergistic neutralization was observed; shaded gray box indicates the area of maximum synergy between the two monoclonal antibodies, and the δ-score for this area is shown. The δ-score is a synergy score: values < -10 indicate antagonism; values -10 to 10 indicate an additive effect; values > 10 indicate synergy. Data in (A-C) are from one experiment performed in technical duplicate.

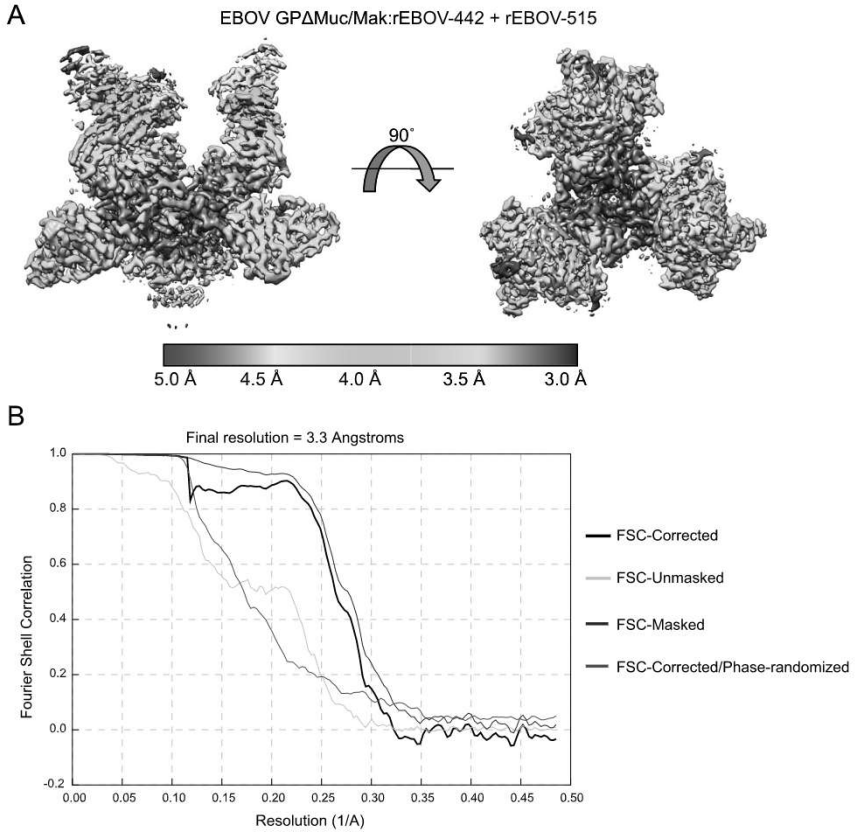

Figure S4. Cryo-EM local resolution estimation and FSC curves, related to Figure 6

(A) The local resolution of the EBOV GPΔMuc/Mak:rEBOV-442/rEBOV-515 cryo-EM map, with local resolutions indicated according to the colors in the legend below.

(B) The Fourier shell correlation (FSC) curve for the EBOV GPΔMuc/Mak:rEBOV-442/rEBOV-515 cryo-EM map, generated by Relion 3.1.

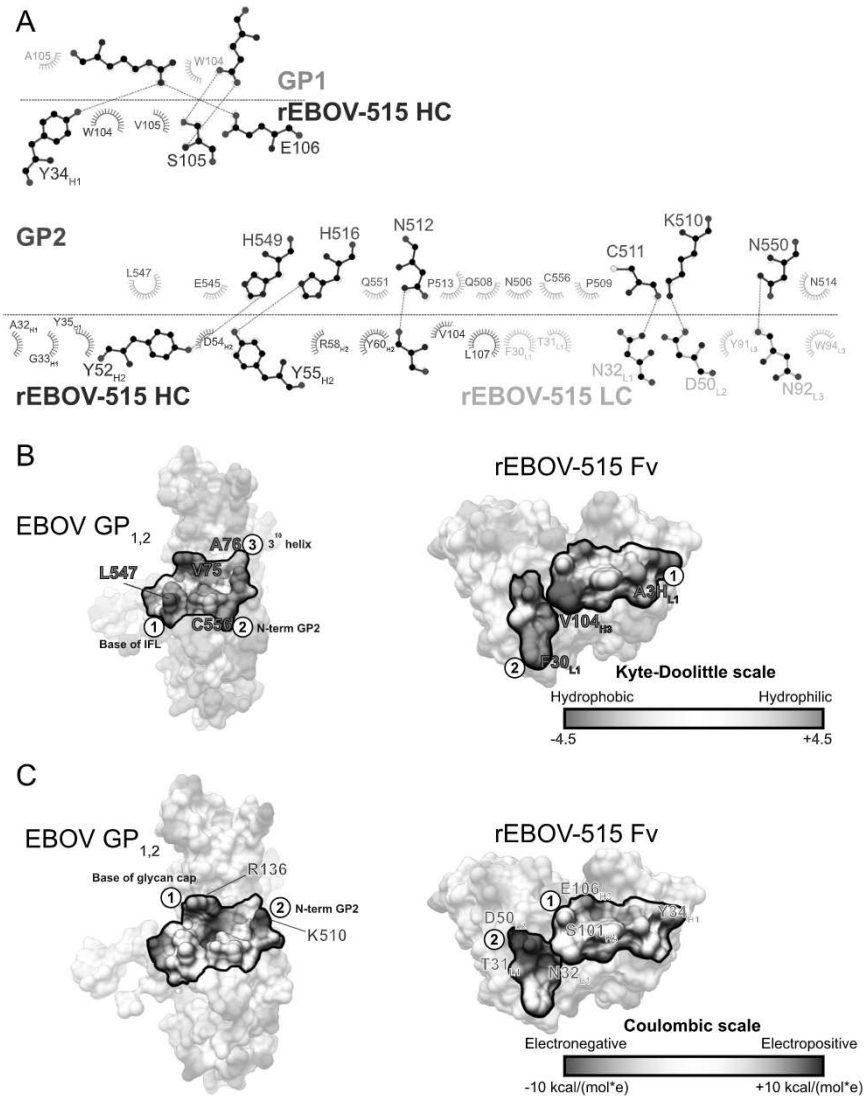

Figure S5. Epitope and paratope binding properties of rEBOV-515, related to Figure 6

(A) LigPlot schematic showing interaction of rEBOV-515 with GP1 (above) or GP2 (below). Residues that make hydrogen bonds are rendered, and those that contribute van der Waals interactions are drawn as semi-circles. rEBOV-515 CDR loop residues are colored according to the labels, with GP residues in magenta/pink and backbone residues colored in dark cyan. Chain identifiers are in parenthesis.

(B) Kyte-Doolittle surface rendering of $GP_{1,2}$ (left) and a face-on view of the rEBOV-515 Fv paratope (right) with the interacting regions highlighted. Key hydrophobic residues are indicated with important regions of interaction labeled 1-3 on the GP epitope and the corresponding interacting residues labeled 1-3 on the rEBOV-515 paratope.

(C) Similar epitope/paratope interaction rendering as in (B) but with Coulombic surface rendering, indicating key electronegative regions on GP that interact with electropositive regions on the rEBOV-515 paratope.

Subunit	Residue number	Total Contacts	Residue	rEBOV-515	rEBOV-520	ADI-15946
GP1	74	8	G	>	6	2
	75	4	V	>	4	>
	77	2	T	>	2	>
	78	3	D	>	3	>
	104	1	W	1	>	>
	106	28	E	12	5	11
	107	7	N	>	7	>
	136	29	R	13	5	11
	137	2	Y	>	2	>
	250	3	P	>	3	>
	251	1	Q	>	1	>
	255	5	Q	>	5	>
GP2	506	8	N	5	>	3
	508	2	Q	1	>	1
	509	2	P	1	>	1
	510	24	K	4	5	15
	511	14	C	4	3	7
	512	29	P	3	14	12
	513	14	N	6	3	5
	514	22	P	6	5	11
	516	9	H	5	2	2
	545	3	E	3	>	>
	547	24	L	13	11	>
	549	20	H	11	3	6
	550	2	N	1	>	1
	556	2	C	2	>	>

Figure S6. Contact residues for broadly reactive antibodies rEBOV-515, rEBOV-520, and ADI-15946, related to Figure 6

Base binding mAb contacts on EBOV GP determined by UCSF Chimera with a default cutoff value of −0.4 Å and an allowance of 0 Å (Pettersen et al., 2004). rEBOV-520 from PDB 6PCI (Gilchuk et al., 2020b), ADI-15946 from PDB 6MAM (West et al., 2019). Gradient is green to red, with green being fewer contacts and red being the most contacts.

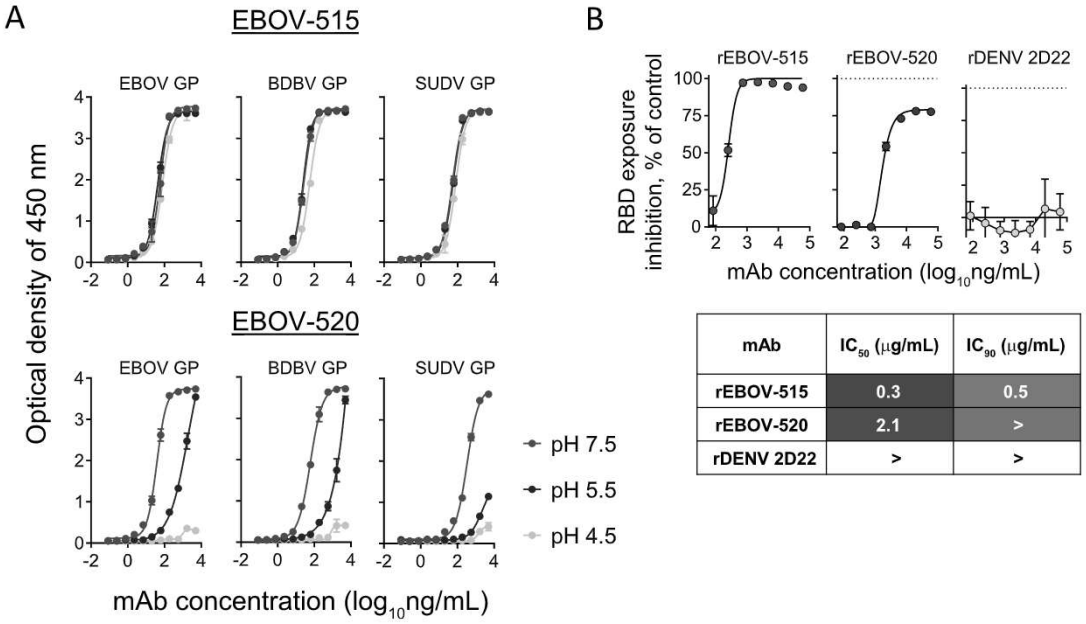

mAb	IC_{50} (μg/mL)	IC_{90} (μg/mL)
rEBOV-515	0.3	0.5
rEBOV-520	2.1	>
rDENV 2D22	>	>

Figure S7. rEBOV-515 retains GP-binding capacity at low pH and efficiently inhibits GP cleavage, related to Figure 6

(A) ELISA binding of rEBOV-515 or rEBOV-520 to the recombinant EBOV, BDBV, or SUDV GP ΔTM at neutral or acidic pH. The mean ± SD of technical triplicates and one of two independent experiments are shown.

(B) Cleavage inhibition by the GP-base specific antibodies. Jurkat EBOV-GP cells were pre-incubated with various concentrations of indicated antibodies, treated with thermolysin, then incubated with fluorescently-labeled mAb MR78 that recognizes the receptor binding site (RBS) of the cleaved EBOV GP, does not bind to uncleaved EBOV GP, and does not compete with rEBOV-515 or rEBOV-520 for EBOV GP_{CL} binding. An unlabeled mAb rDENV 2D22 was used as control for non-inhibitory mAb activity. Results are expressed as the percent of inhibition of RBS exposure in the presence of tested mAb relative to controls for minimal binding of labeled MR78 mAb-only to intact (uncleaved) Jurkat EBOV-GP, and maximal binding of labeled MR78 mAb-only to cleaved Jurkat-EBOV GP. Mean ± SD of technical triplicates and one of two independent experiments are shown.